Unravelling the sources of uncertainty in glacier runoff projections in the Patagonian Andes (40–56° S)

Rodrigo Aguayo[1,2], Fabien Maussion[3,4], Lilian Schuster[3], Marius Schaefer[5], Alexis Caro[6], Patrick Schmitt[3], Jonathan Mackay[7,8], Lizz Ultee[9], Jorge Leon-Muñoz[10,11,12], and Mauricio Aguayo[1]

[1]Centro EULA, Facultad de Ciencias Ambientales, Universidad de Concepción, Concepción, Chile.
[2]Department of Water and Climate, Vrije Universiteit Brussel, Brussels, Belgium
[3]Department of Atmospheric and Cryospheric Sciences (ACINN), Universität Innsbruck, Innsbruck, Austria
[4]School of Geographical Sciences, University of Bristol, Bristol, UK
10 [5]Instituto de Ciencias Físicas y Matemáticas, Universidad Austral de Chile, Valdivia, Chile
[6]Univ. Grenoble Alpes, CNRS, IRD, INRAE, Grenoble-INP, Institut des Géosciences de l'Environnement, Grenoble, France
[7]British Geological Survey, Keyworth, Nottingham, United Kingdom
[8]School of Geography, Earth and Environmental Sciences, University of Birmingham, Edgbaston, Birmingham, UK
[9]Department of Earth & Climate Sciences, Middlebury College, Middlebury, US
15 [10]Departamento de Química Ambiental, Universidad Católica de la Santísima Concepción, Concepción, Chile
[11]Centro Interdisciplinario para la Investigación Acuícola (INCAR), Concepción, Chile
[12]Centro de Energía, Universidad Católica de la Santísima Concepción, Concepción, Chile

Correspondence to: Rodrigo Aguayo (rodaguayo@udec.cl)

Abstract. Glaciers are retreating globally and are projected to continue to lose mass in the coming decades, directly affecting downstream ecosystems through changes in glacier runoff. Estimating the future evolution of glacier runoff involves several sources of data uncertainty, which to date have not been comprehensively assessed on a regional scale. In this study, we used the Open Global Glacier Model (OGGM) to estimate the evolution of each glacier (area > 1 km^2) in the Patagonian Andes
25 (40–56° S), which are distributed in 847 catchments covering 9 different hydrological zones. We used different glacier inventories (n = 2), ice thickness datasets (n = 2), historical climate datasets (n = 4), general circulation models (GCMs; n = 10), emission scenarios (SSPs; n = 4), and bias correction methods (BCMs; n = 3) to generate 1,920 possible scenarios over the period 1980–2099. In each scenario, glacier runoff and melt time series were characterised by ten glacio-hydrological signatures (i.e., metrics). We used the permutation feature importance of random forest regression models to assess the relative
30 importance of each source on the signatures of each catchment. Considering all scenarios, 34% ± 13% (mean ± one standard deviation) of the glacier area has already peaked in terms of glacier melt (year 2020), and 68% ± 21% of the glacier area will lose more than 50% of its volume this century. Considering the glacier melt signatures, the future sources of uncertainty (GCMs, SSPs and BCMs) were the main source in only 17% ± 21% of the total glacier area. In contrast, the reference climate was the main source in 69% ± 22% of the glacier area, highlighting the importance of the choices we make in the calibration
35 procedure. The results provide a basis for prioritizing future efforts (e.g., improve reference climate characterisation) to reduce glacio-hydrological modelling gaps in poorly instrumented regions such as the Patagonian Andes.

1 Introduction

Glaciers are retreating worldwide (Hugonnet et al., 2021) and are projected to continue to lose mass (Marzeion et al., 2020). Recent projections by Rounce et al. (2023) indicate that glaciers will lose 26 ± 6% (+1.5 °C) to 41 ± 11% (+4 °C) of their present mass by 2100 (median ± 95% confidence interval), contributing between 90 ± 26 and 154 ± 44 mm to sea-level rise, respectively. The rapid glacier shrinkage has led to cascading effects on downstream systems (Huss et al., 2017; Milner et al., 2017), affecting the availability and quality of water resources (IPCC, 2022), and causing changes in the ecological (Cauvy-Fraunié and Dangles, 2019) and socio-economic (Rasul and Molden, 2019) aspects of downstream environments.

One of the most important impacts of glaciers on downstream systems is the contribution of meltwater to streamflow (Huss and Hock, 2018), which is essential for irrigation, industry, domestic use, hydropower and ecosystems (Immerzeel et al., 2020; Viviroli et al., 2020). However, as glaciers continue to shrink, the reliability and quantity of this water reserve becomes increasingly uncertain, potentially increasing drought stress (Kaser et al., 2010; Pritchard, 2019; Van Tiel et al., 2021, 2023). Ultee et al. (2022) showed globally that accounting for glacier runoff reduces simulated drought frequency and severity, even in basins with low glacier cover (< 2%). The buffering effect is higher in moderately glaciated arid regions, such as the Central Andes, and is projected to increase through the 21st century. In this region, glaciers have provided an important drought mitigation capacity during the current Mega Drought (Ayala et al., 2020; McCarthy et al., 2022), which is unprecedented in recent centuries according to dendrochronological studies (Garreaud et al., 2017; Morales et al., 2020).

Recent global estimates suggest that Andean glaciers are likely to be one of the largest per unit area contributors to sea level rise, with a contribution of 0.057 ± 0.006 mm SLE yr^{-1} (-20.7 ± 2.1 Gt yr^{-1}) representing 7.7% of the global mass loss between 2000 and 2019 (mean ± 95% confidence interval) (Hugonnet et al., 2021). Glaciers in the Patagonian Andes account for 96% of the total ice loss in the Southern Andes (Braun et al., 2019), which has accelerated in recent decades (Davies and Glasser, 2012; Dussaillant et al., 2019). Due to the high precipitation levels in the Patagonian Andes (Aguayo et al., 2024), the contribution of glaciers to regional water supply is generally low, with glacier runoff serving as a flow buffer during dry periods rather than a major source of streamflow (Ruiz et al., 2022). Nevertheless, recent studies have reported increased flows in rivers with important glacier cover (Masiokas et al., 2019; Vries et al., 2023), some of which have only begun to show significant trends (p < 0.01) in the last decade (e.g., Santa Cruz; Pasquini et al., 2021).

Despite efforts to improve the understanding of glacier processes in the Patagonian Andes, there are still important limitations due to the lack of ground-based validation data. To address these limitations, many modelling studies have used dynamic and/or statistical downscaling methods based on climate reanalyses (Table S1). However, the different approaches and data sources have overestimated the precipitation according to numerical simulations of regional moisture fluxes (Sauter, 2020). Despite the severe lack of data on melt patterns and snow accumulation in the upper plateaus of the Patagonian Icefields (Bravo

et al., 2019a, b), most regional modelling efforts have focused on this region (Table S1). In this area, glacier modelling has generally relied on energy balance approaches based on downscaled reanalysis data. Only two studies have modelled the regional hydrological contribution of the Patagonian glaciers. Using the SnowModel (1979-2014), Mernild et al. (2017) estimated a mean specific runoff of 6,240 and 6,700 mm yr^{-1} for the SPI and NPI, respectively. More recently, Caro et al. (2024) used the Open Global Glacier Model (OGGM) to compare the hydrological response of Andean catchments between 2000-2009 and 2010-2019. In the Patagonian Andes, an increase in glacier melt was found, ranging from 6% to 14% depending on the zone. Although recent modelling efforts have benefited from the increased availability of geodetic mass balances to calibrate and validate surface mass balance models (Table S1), important sources of uncertainty in the future evolution of Patagonian glaciers remain.

There are several sources of uncertainty in the modelling chain of glacier projections. At the global scale, results from the Glacier Model Intercomparison Project Phase 2 (GlacierMIP2) showed that the emission scenario is the largest source of uncertainty by the end of the century, but the uncertainty from the glacier models, which use different data sources and calibration setups, is the largest source until 2050 (Marzeion et al., 2020). Locally, several studies have shown that individual choices during model initialization and calibration, such as the historical climate (Compagno et al., 2021; Watanabe et al., 2019), the glacier inventory (Li et al., 2022), the ice thickness (Gabbi et al., 2012), and the downscaling strategy (Schuster et al., 2023), have an impact on glacier evolution. However, few studies have examined the influence of multiple components of the modelling chain on projected glacio-hydrological changes. Huss et al. (2014) found that winter snow accumulation and the glacier retreat model have the greatest influence on the glacier runoff projections in the Findelengletscher basin (Switzerland), while the downscaling strategy, calibration data quality and the surface mass balance model are of secondary importance. Mackay et al. (2019) used hydrological signatures, which are quantitative metrics that describe the dynamic properties of hydrological time series (McMillan, 2021), to measure changes in the hydrology of the Virkisá basin (southern Iceland). They found that the main source of uncertainty were the climate model chain components (global circulation models and emission scenarios), but for certain hydrological signatures the most important source was the representation of glacio-hydrological processes. Overall, adding additional data (e.g., snow cover area, glacier mass change) to the calibration of glacio-hydrological processes has shown to be more important than increasing the complexity of the model (Van Tiel et al., 2020).

In this study, we investigated the importance of six sources of data uncertainty in ten glacio-hydrological signatures (i.e., metrics) that characterise the evolution of glacier runoff . The sources of uncertainty were glacier inventories (n = 2), ice thickness datasets (n = 2), historical climates (n = 4), global circulation models (n = 10), emission scenarios (n = 4) and bias correction methods (n = 3). The scenarios were tested using the Open Global Glacier Model (OGGM) to project the evolution of each glacier (area > 1 km^2) in the Patagonian Andes (40–56° S) over the period 1980–2099. Finally, the importance of each source of data uncertainty was measured using the permutation feature importance of random forest regression models.

2 Study area

Our study area comprises the Patagonian Andes (40–56º S; Fig. 1), where the seasonal melting of glaciers is essential for the long-term sustainability of the local ecosystems and coastal human populations (Iriarte et al., 2014). Glaciers in the Patagonian Andes cover an extensive area of 25,886 km^2, which represents 82% of the total glacierized area of the Andes at the time of the inventory (year ~2000; RGI Consortium, 2017). This region includes the Northern and Southern Patagonian Icefields (NPI and SPI), which form the largest freshwater reservoir in the Southern Hemisphere outside of Antarctica, with a total area of 17,195 km^2 in 2011 (Davies and Glasser, 2012), and an estimated ice volume of 4,756 ± 923 km^3 (Millan et al., 2019).

We selected 847 glacierized catchments, each with at least one glacier and a glacier area greater than 0.1%. The 0.1% glacier area threshold was selected as a conservative threshold for drought buffering effect (see Fig. 3 in Ultee et al. 2022). The catchments were aggregated into nine hydrological zones (Fig. 1), which were selected based on the spatial patterns of precipitation and temperature that showed a strong capacity to reproduce recent glacier changes (Caro et al., 2021). The northern area (~ 41–46º S; Fig. 1) is characterized by two zones that aggregate large catchments with a low glacier area: Petrohue, Puelo and Yelcho (PPY) basins, and Palena, Cisnes and Aysen (PCA) basins. The Northern Patagonian Icefield (NPI; ~ 46–48º S) was divided into two zones according to its main aspect (NPI-E and NPI-W). The eastern side (NPI-E) coincides with the location of the Baker River Basin, one of the catchments with the largest glacier area in the study area and the focus of regional (Dussaillant et al., 2019) and global (Huss and Hock, 2018) glacio-hydrological studies. The Southern Patagonian Icefield (SPI; ~ 48–52º S) was divided latitudinally according to the main catchments on the eastern side (Pascua in SPI-N, Santa Cruz in SPI-C and Grey in SPI-S). Finally, the southern area was divided into the Gran Campo Nevado (GCN; ~ 52–54º S) and the Cordillera Darwin Icefield (CDI; < ~ 54º S), which hosts many small catchments. In contrast to the rest of the area, both southern zones receive uniform precipitation throughout the year, with no clear seasonality.
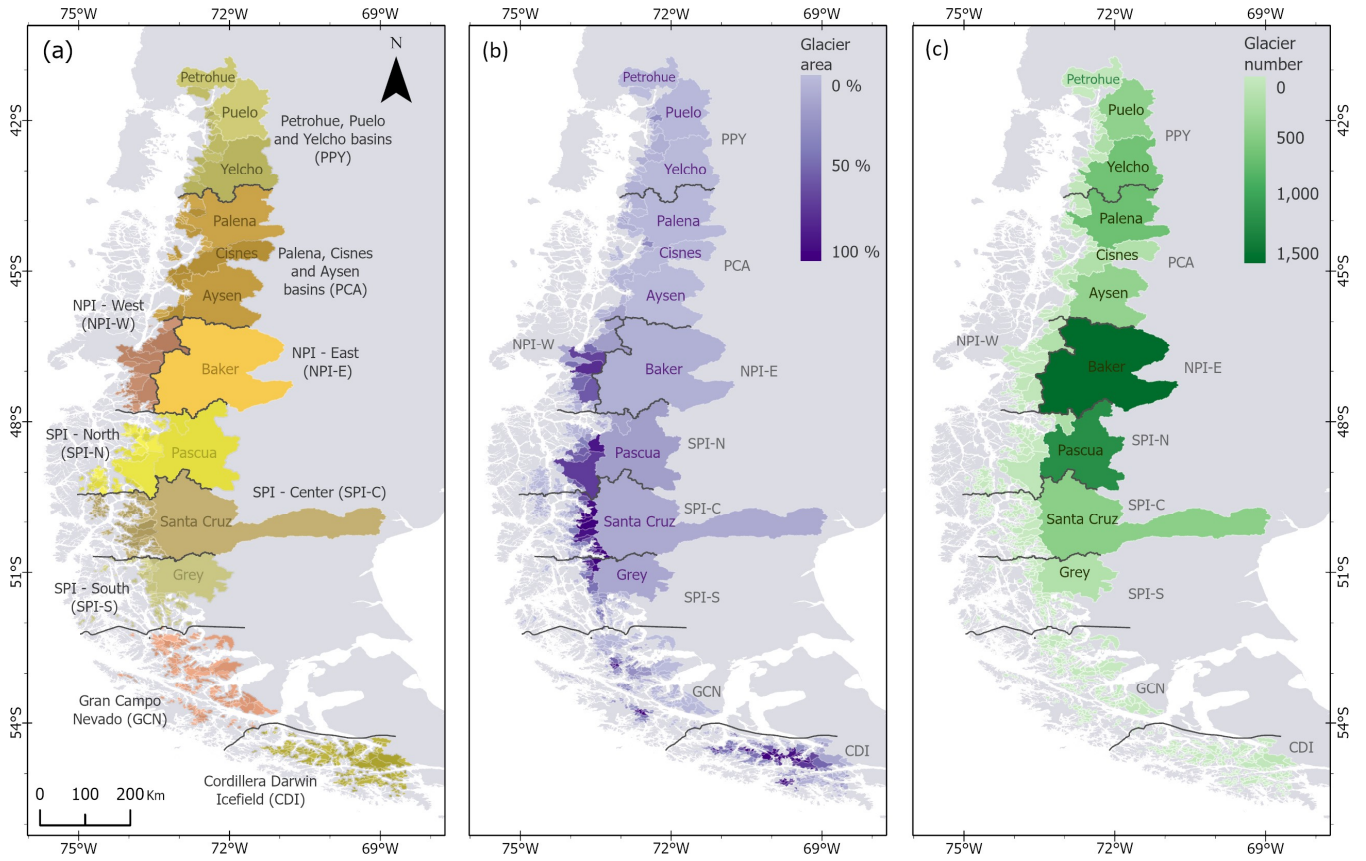
Figure 1. Study area. a) Hydrological zones (n = 9) for the 847 catchments. The names in grey correspond to the names of the main catchments (area > 5,000 km², in the study area, which account for the 68% of the total catchment area. b) Glacier area for each catchment. c) Number of glaciers in RGI6 per catchment.

3 Methods

3.1 The Open Global Glacier Model (OGGM)

We used the Open Global Glacier Model v1.5.4 (OGGM, Maussion et al., 2019) to model the evolution of all the glaciers in the study area. OGGM is an open-source model that couples a surface mass balance model with a model of glacier dynamics. The model has been used in global studies (Marzeion et al., 2020; Rounce et al., 2023; Zekollari et al., 2024) and hydrological studies (e.g., Caro et al., 2024; Hanus et al., 2024; Pesci et al., 2023; Zhao et al., 2023). The climatic mass balance model is based on an extended version of the temperature-index model used by Marzeion et al. (2012). In this approach, the monthly mass balance (B_i) at elevation z is calculated as:

$$B_i(z) = P_f \cdot P_i^s(z) \ - \mu^* \cdot \max(\,T_i(z) - T_{melt},\ 0), \tag{1}$$

130   where P_f is a precipitation factor used to account for measurement biases in mountainous topography, to further downscale precipitation to the glacier resolution, and to account for missing processes (e.g., debris cover, firn densification, avalanches) not explicitly included in the mass balance. P_i^s and T_i are the monthly solid precipitation and air temperature, μ^* is the temperature sensitivity of the glacier, and T_{melt} is the monthly mean air temperature above which ice melt is assumed to occur. The climate variables are obtained from the nearest grid point. In the case of temperature, this is adjusted to the glacier surface

135   elevation using a constant lapse rate of -6.5 ℃ km^{-1}, a value commonly used in the study area (Table S1). Positive degree-months and solid precipitation are calculated using the default thresholds for melting (T_{melt} = -1 ℃) and accumulation (T_{solid} = 0 ℃ and T_{liquid} = 2 ℃). When the temperature is between T_{solid} and T_{liquid}, the solid precipitation varies linearly between 100% and 0% at the lower and upper limits, respectively. The contributions of positive degree-months and solid precipitation are combined to calculate the monthly mass balance, which is used to update the glacier geometry annually.

140   Gridded glacier geometry is obtained by overlaying glacier inventory outlines and NASADEM elevation data (NASA JPL, 2020) on a regular grid. The resolution of the grid varies with the glacier size, ranging from 10 to 200 m. Glaciers are then segmented into elevation bands, each of which covers an elevation difference of 30 m, following the algorithm described in Werder et al. (2020). The ice dynamics flowline model of OGGM relies on a depth-integrated ice velocity u (m s^{-1}), utilizing the shallow ice approximation (SIA):

$$u = \frac{2A}{n+1} \cdot h \cdot (\rho \cdot g \cdot h \cdot \alpha)^n, \tag{2}$$

145   where A is the ice creep parameter (s^{-1} PA^{-3}), n is the exponent of Glen's flow law (n=3), h is the local ice thickness (m), ρ is the ice density (900 kg m^{-3}), g is the gravitational acceleration (9.81 m s^{-2}), and α is the surface slope computed numerically along the flowline (following Eq. 3 and 4 of Maussion et al. 2019). With this velocity, the flux of ice along the glacier is explicitly computed.

      In this study, we set the precipitation factor (P_f) to 1.0 to assess the influence of different reference climates on the evolution

150   of each glacier (Fig. 2), assuming that the estimated precipitation from the different products corresponds to the "true" values. Frontal ablation of marine-terminating and lake-terminating glaciers was not explicitly simulated. However, Malles et al. (2023) recently showed that the mass-balance model (through different temperature sensitivities) implicitly accounts for the effect of frontal ablation when calibrated against the Hugonnet et al. (2021) observations, resulting in relatively small changes in the projections. This is an acknowledged shortcoming of our study and should be further investigated in future studies.

155   The calibration of each glacier consisted of a newly developed iterative process that involves three parameters: the temperature sensitivity (μ^*; Eq. 1), the composite ice creep parameter (A; encapsulating basal sliding and ice deformation, Eq. 2) , and

finally, the spin-up temperature (T_{spinup}; used to find a historical glacier state). The calibration procedure, shown in Fig. 2, unfolds through the following steps:

i. Define the initial value of μ^* (Eq. 1) by matching the modelled specific mass balance with the geodetic mass balance of Hugonnet et al. (2021). This is calculated using the period 2000 to 2020, the reference climate and the static surface geometry, which refers to the outline obtained from the Randolph Glacier Inventory (RGI; see next section).

ii. Compute an apparent mass balance using the static surface geometry and the reference climate in the geodetic mass balance period (2000–2020). The apparent mass balance is defined as the specific mass balance plus a residual term, which shifts the complete mass balance profile. This adjustment ensures that the resulting specific mass balance is zero, following the equilibrium assumption in the inversion process described by Maussion et al. (2019).

iii. Use the derived apparent mass balance for an inversion for the underlying glacier bed. Throughout this inversion, parameter A (Eq. 2) is defined such that the resulting inversion glacier volume matches the estimates for each hydrological zone defined in Fig. 1. The inversion method follows Maussion et al. (2019) when the sliding parameter is set to 0.

iv. The next step is to find a glacier state in the past (first attempt 1980) from which a dynamic glacier run to the RGI date (approx. year 2000) results in the given RGI area. To define different glacier states in the past, the temperature spin-up T_{spinup} (first guess is -1 °C) is added to the reference climate and we define a mean mass balance using the reference climate between 1980 and the RGI date. With this mean mass balance a 20-year dynamic model run is conducted and the resulting glacier state defines the 1980 extent. How consecutive guesses of T_{spinup} are found is described in Appendix A. If the resulting glacier is too large even when we start from an ice-free initial glacier state in the past, or the resulting glacier is too small and the algorithm grows the glacier outside the domain, a shorter spin-up period is tried two times (starting in 1985 or 1990). If the spin-up period is shortened, a fixed geometry volume is calculated by going backwards to 1980, using the calculated mass change on the constant surface geometry (assuming a bulk density of 900 kg m^{-3}). This is done to have a continuous volume time-series for all glaciers. We only move on if this step has successfully found a proper past glacier state to match the RGI area within 1 km^2 or 1% of the total area, whatever is smaller.

v. Initiate a dynamic simulation from 1980 to 2020, using the reference climate inputs and starting from the glacier state inferred in the previous step.

vi. Finally, the geodetic mass balance resulting from the dynamic simulation is calculated and compared with the observed values from Hugonnet et al. (2021). If the difference between these values is within the defined uncertainty (±250 kg m^{-2} yr^{-1}), the calibration/initialization workflow is terminated and the resulting glacier in 2020 and the parameters μ^* and A

are used as inputs for the projection runs. If not, a new µ* is defined (Appendix A) and the process starts again from the beginning.
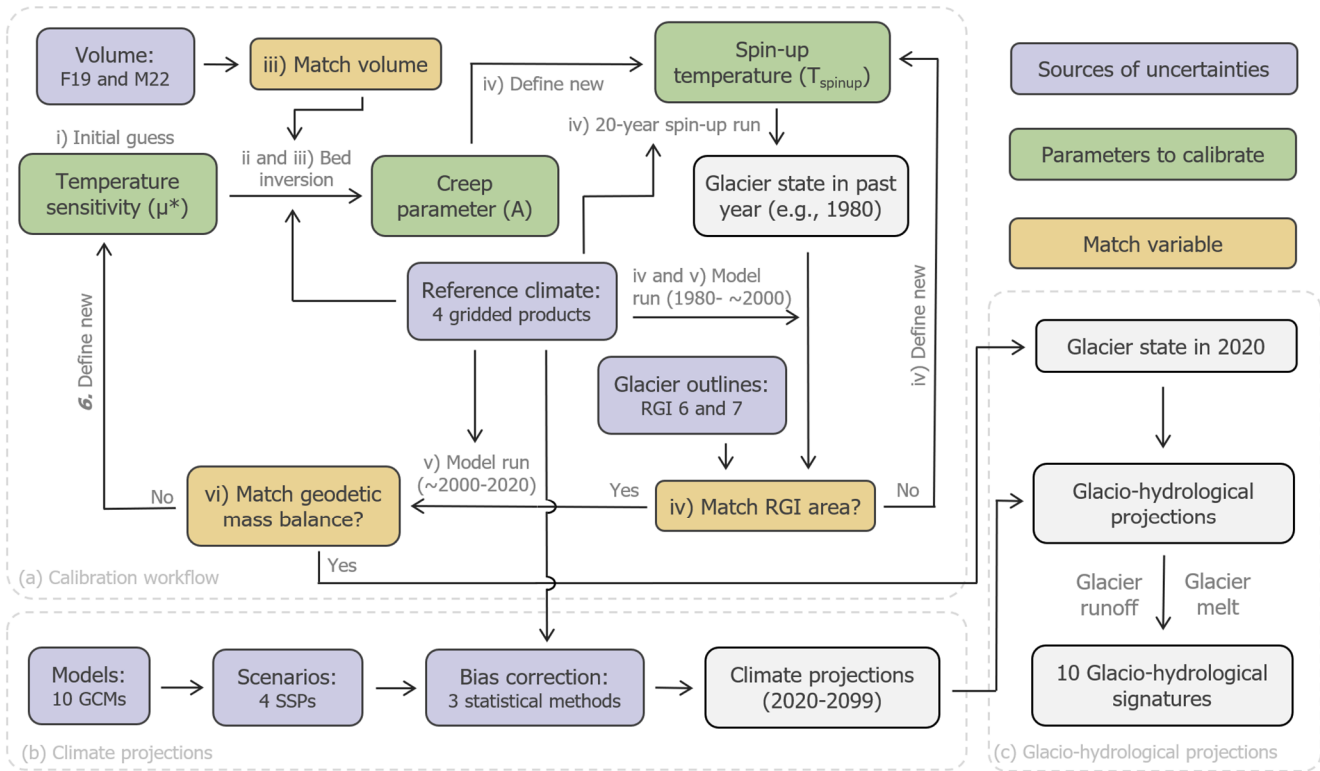
Figure 2. Methodological framework. a) Open Global Glacier Model (OGGM) dynamic calibration workflow. Roman numerals refer to the calibration steps in Section 3.1. b) Climate projections. c) Glacio-hydrological projections. GCM: General Circulation Models. SSP: Shared Socioeconomic Pathways. F19 and M22: Thickness estimated from Farinotti et al. (2019) and Millan et al. (2022). RGI: Randolph Glacier Inventory.

3.2 Sources of uncertainty

3.2.1 Geometry and volume

The geometry, represented by the glacier outlines, was obtained from RGI6 (Randolph Glacier Inventory - Version 6) (RGI Consortium, 2017) and RGI7 (RGI Consortium, 2023). In the latest version, RGI7 integrates the national inventories of Chile (Barcaza et al., 2017) and Argentina (Zalazar et al., 2020). Previous assessments of the complete RGI region (20–56º S) have shown that both datasets (RGI6 and RGI7) show similar areas across different latitudes (-3% of total area relative to RGI6; Zalazar et al., 2020). Nevertheless, the national inventories included in RGI7 showed a higher number of glaciers ($\Delta n = 8,493$) and area ($\Delta = 651$ km^2) for the smallest glaciers (< 0.5 km^2), and differences of less than 7% in the Patagonian Icefields compared to RGI6.

Individual volumes for each glacier were derived from the thickness estimated from Farinotti et al. (2019) and Millan et al.
(2022) (hereafter F19 and M22, respectively). F19 is a consensus estimate from five models that use principles of ice flow
dynamics to infer ice thickness from surface properties. In contrast, M22 uses glacier flow mapping to reconcile the spatial
distribution of ice masses with glacier dynamics, morphology, and ice divides. In the southern Andes, Hock et al. (2023)
reported that M22 had 13% more total ice volume than F19. Considering that the two volume data sources do not have a
complete coverage of all glaciers in RGI6 (100% and 98.2% of the area for F19 and M22, respectively) and RGI7 (99.1% and
96.4% of the area for F19 and M22, respectively), we used a volume-area scaling (VAS, Hock et al., 2023) to complete the
coverage. In this approach, we calculated the VAS parameters for each hydrological zone (defined in Fig. 1) and volume data
source separately.

3.2.2 Reference historical climate (1980–2015)

We used monthly precipitation and air temperature time series from ERA5 (0.25º; Hersbach et al., 2020) and three gauge-
corrected alternatives that use ERA5 in the bias correction process (CR2MET v2.5, MSWEP v2.8/MSWX and PMET v1.0).
CR2MET v2.5 (0.05º; Boisier, 2023) is the current national reference for hydrometeorological studies in Chile, and is based
on a statistical downscaling technique that uses ERA5, meteorological records, satellite land surface temperature and
topographic descriptors. MSWEP v2.8 (0.1º; Beck et al., 2019) is a global precipitation product that merges gauges, satellites
and reanalysis data, and has outperformed other state-of-the-art precipitation products over Chile (Zambrano-Bigiarini, 2018).
Precipitation from MSWEP v2.8 was complemented with air temperature from MSWX (0.1º; Beck et al., 2022), a bias-
corrected meteorological product compatible with MSWEP. Finally, PMET v1.0 (Aguayo et al., 2024) was developed for
Western Patagonia using statistical bias correction procedures, spatial regression models (random forest), and hydrological
methods (Budyko framework) to correct the underestimation of precipitation reported in areas with pronounced elevation
gradients and significant snowfall. PMET outperformed ERA5, CR2MET and MSWEP in terms of hydrological modelling
performance (Aguayo et al., 2024).

3.2.3 Climate projections (2020–2099)

Climate projections of monthly precipitation and air temperature were obtained from 10 General Circulation Models (GCMs,
Table S2) of the Coupled Model Intercomparison Project 6 (CMIP6; Eyring et al., 2016). Previous hydrological studies have
suggested that 10 GCMs can ensure that the median of all possible combinations produces similar uncertainty components as
the entire ensemble (Wang et al., 2020). Considering only GCMs with at least one output in all emission scenarios, the selection
of the 10 GCMs was based on the recommendations of Hausfather et al. (2022), who suggest focusing on a subset of GCMs
that are most consistent with the assessed warming projections of the Sixth Assessment Report (AR6). In this case, the selected
GCMs have a transient climate response (TCR; temperature change at the time of CO_2 doubling) that lies in the "likely" range
of 1.4 - 2.2 °C (Table S2), which is a good approximation of the assessed warming (Tokarska et al., 2020). Considering that

235   future scenarios are the main source of uncertainty at the end of the century in the southern Andes (Marzeion et al., 2020), we used four different Shared Socioeconomic Pathways (SSPs; O'Neill et al., 2016): SSP1-2.6, SSP2-4.5, SSP3-7.0 and SSP5-8.5. Each GCM was initially resampled to 1.0º using a bilinear filter, and only the standard model realisation was considered (r1i1p1f1 in all cases).

3.2.4 Bias correction method

240   Three statistical bias correction methods were evaluated to assess their impact on the glacier projections. The objective of bias correction is to minimize the systematic error of the climate projections obtained from general circulation models (Section 3.2.3) using the reference climate used in the calibration process (Section 3.2.2). The selected methods were: Mean and Variance Scaling (MVA; Chen et al., 2011), Quantile Delta Mapping (QDM; Cannon et al., 2015) and Multivariate Bias Correction with N-dimensional probability density function transformation (MBCn; Cannon, 2018). The MVA approach was

245   commonly used in GlacierMIP2, as it guarantees that the bias-corrected time series has the same mean and variance as the reference time series in the reference period. QDM is a hybrid method that combines quantile-based delta change and bias correction methods. Thus, it not only preserves the quantile changes predicted by climate projections, but also corrects the biases of the modelled series with respect to those of the reference time series. Finally, MBCn is a multivariate bias correction that has the advantage of transforming all aspects of the reference multivariate distribution to the multivariate distribution

250   simulated by the climate models. The bias correction parameters of all methods were calculated on a monthly basis to account for the seasonality of GCM biases. Following the protocol of the Inter-Sectoral Impact Model Intercomparison Project (ISIMIP3b; Lange, 2021), the reference period was 1980–2015 for all correction methods. Climate outputs based on the QDM and MBCn approaches were obtained using the *xclim* package v0.4 (Logan et al., 2022).

3.3 Comparative analysis of sources of uncertainty

255   Taking all glaciers into account, each source of data uncertainty was analysed to quantify the difference between the alternatives. For area and volume, we calculated the relative and absolute differences for each catchment and hydrological zone defined in Fig. 1. To calculate these differences, we aggregated glacier area and volume for a given catchment by selecting all glaciers with their terminus location within that catchment. It is assumed that, if the inventory outlines are correct, all the water flowing out of the glacier will flow via its terminus. In addition, we compared the acquisition dates of the glacier

260   geometries for both inventories. To assess the influence of the reference climate on the glacier mass balance, we calculated the solid precipitation and positive degree-day sum in addition to precipitation and temperature. To isolate the effect of the spatial resolution, temperature from ERA5 and MSWEP/MSWX was downscaled to 0.05º using the same lapse rate used by OGGM (-6.5 ℃ km^{-1}). Precipitation was not downscaled. Similarly, solid precipitation and positive degree-day sum were calculated using the thresholds indicated in Section 2.1 (T_{melt} = -1 ℃, T_{solid} = 0 ℃ and T_{liquid} = 2 ℃). Specifically, we calculated and

compared annual means for each variable, catchment, and product for the reference period (1980–2015) using only the glacierized grid cells.

The climate projections were another source of uncertainty. To assess the impact of the raw climate projections, we calculated the relative change between the reference period (1980–2015) and the future period (2070–2099) for each GCM and SSP. In addition, we calculated the model agreement of precipitation following Iturbide et al. (2021), who defined a high model agreement when more than 80% of the GCMs agree on the sign of the change. Finally, to assess the individual impact of each climate uncertainty source, we calculated the standard deviation across different reference climates, GCMs, SSPs, and bias correction methods. Specifically, we calculated the standard deviation based on the long-term annual mean of each variable, catchment, and alternative. Analogous to the reference climate, we calculated the annual mean for the future period (2070-2099) using only the glacierized grid cells.

3.4 Glacio-hydrological runs

We used the OGGM model to estimate the evolution over the period 1980–2099 of all glaciers with an area > 1 km^2 in the Patagonian Andes (40–56° S). This corresponds to 2,034 and 1,837 glaciers that accumulate 99.0% and 98.5% of the total volume estimated by Millan et al. (2022) for RGI6 and RGI7, respectively. For each glacier, we evaluated 16 scenarios generated by the historical sources of uncertainty: glacier outlines (n = 2), volume datasets (n = 2) and reference climates (n = 4). These scenarios were used to project the future evolution given by different GCMs (n = 10), future scenarios (n = 4), and bias correction methods (n = 3), resulting in 120 future scenarios for each historical simulation (a total of 1920 potential scenarios; Fig. 2). To estimate the glacier volume that is unsustainable under current conditions, we additionally ran 16 simulations for 80 years with a pseudo-random climate based on the historical climate (30 years) around the year 2000.

For all 1920 scenarios, we extracted the annual glacier area, volume, and specific mass balance of each modelled glacier. To assess the hydrological contribution, we additionally extracted glacier runoff which corresponds to all water originating from the initially glacierized area (i.e., here year 1980; Huss and Hock, 2018). In this approach, OGGM calculates the glacier runoff from the sum of on- and off-glacier melt and on- and off-glacier liquid precipitation. To disaggregate the impact of projected precipitation changes, we also extracted the melt on glacier (hereafter glacier melt), which is the sum of ice and seasonal snow melt on the glacier (Fig. 2c). As in the comparative analysis (Section 3.3), the time series were initially aggregated at the catchment scale according to the location of the glacier terminus.

Glacier runoff and melt were characterised by 10 glacio-hydrological signatures (i.e., metrics) to describe the hydrological dynamic properties of each catchment (Table 1). The set of signatures was selected to cover the different categories proposed by Richter et al. (1996): magnitude, timing, frequency, duration, and rate of change. Poff et al. (1997) used these categories to characterize the hydrological regime and proposed that these components fully describe the streamflow characteristics that are

important to the aquatic ecosystem. However, our analysis of glacier runoff should not be considered as downstream streamflow because our simulations considered only the initially glacierised area and did not include the interaction with other hydrological fluxes (e.g., evaporation and infiltration).

Table 1. Glacio-hydrological signatures used to characterize glacier runoff and melt time series of each catchment. The regime characteristics corresponds to the initial categories proposed by Richter et al. (1996).

Signature or metric	Regime characteristics	Description	Period	Units
Reference magnitude	Magnitude	Annual mean value (runoff and melt). The value was normalized by the catchment area.	1980–2015	mm yr^{-1}
Peak water year	Timing	Following Huss and Hock (2018), the peak water year was calculated using an 11-year moving average.	1980–2099	date (year)
Peak water magnitude	Magnitude Timing	Maximum annual value in the peak water year. The value was normalized by the catchment area.	1980–2099	mm yr^{-1}
Peak water duration	Duration Timing	Number of years in which the annual value is greater than 90% of the peak water magnitude	1980–2099	years
Inter-annual variability	Frequency	Standard deviation of the detrended and normalized time series. For the detrending, we used the same 11-year moving average.	1980–2099	mm yr^{-1}
Reference seasonal contribution	Duration Magnitude	Percentage of annual runoff that occurs during the summer season (DJF).	1980–2015	%
Reference seasonal variability	Frequency	Standard deviation of the percentage of the annual runoff that occurs during the summer season (DJF).	1980–2015	%
Seasonal shift	Timing Rate of change	Absolute change in summer contribution (DJF) between the reference period and the end of the 21st century	1980–2015 vs. 2070–2099	%
Long-term trend	Timing Rate of change	Indicator of the long-term decline after reaching the peak water. The indicator is defined as the slope between the peak water year and 30 years later.	1980–2099	% dec^{-1}
Long-term change	Rate of change Magnitude	Relative change between reference magnitude and magnitude at the end of the 21st century	1980–2015 vs. 2070–2099	%

3.5 Hydrological importance of sources of uncertainty

We build random forest (RF) regression models based on the six sources of uncertainty to predict the glacio-hydrological signatures of each catchment (Table 1). For this analysis, we selected 329 catchments with at least one glacier (area > 1 km^2) in both inventories. RF regression models generate predictions using an adaptation of Leo Breiman's random forest algorithm, a supervised machine learning method (Breiman, 2001; Svetnik et al., 2003). We used the permutation feature importance to assess the influence of each source (Breiman, 2001). This technique measures the change in model performance (in this case, the Root Mean Square Error; RMSE) after the values of a single model feature have been permuted (also known as shuffled),

with more important features resulting in greater decreases in performance when permuted. This method has been successfully used as a sensitivity analysis tool in several studies (e.g., Bennett et al., 2022; Schmidt et al., 2020). For each catchment and signature, the training set was selected to be 90% of the full dataset of scenarios, and the remaining 10% was used to measure

310   the permutation importance. The importance of each feature (in this case, categorical predictors) was represented as the percentage of the average change in the RMSE over 30 experiments of shuffling one feature. For all RF models, we used 500 regression trees as an ensemble, with each tree having a minimum leaf size of five. For each split, two variables were randomly selected as candidates. The complete procedure was performed using Scikit-learn v1.3.0 (Pedregosa et al., 2011).

4 Results

315   ### 4.1 Analysis of sources of uncertainty

4.1.1 Historical conditions (1980–2015)

The historical conditions involved in the calibration process considered the geometry obtained from the glacier inventories (RGI6 and RGI7), the volume obtained from ice thickness datasets (F19 or M22), and the reference climate dataset (PMET, CR2MET, ERA5 and MSWEP). The incorporation of national inventories in RGI7 resulted in important differences compared

320   to RGI6 (Fig. 3). The total number of glaciers increased from 10,544 in RGI6 to 21,285 in RGI7. Relative to this, RGI6 showed a higher number of glaciers with an area greater than 1.0 km^2, but RGI7 has considerably more smaller glaciers (< 1.0 km^2). The total glacier area decreased by 4.0% in RGI7 ($\Delta = 1,024$ km^2), with important regional differences (Fig. 3a,b). The northern area between the Puelo and Aysen catchments (PPY and PCA) showed increases ranging from 4% to 15% relative to RGI6 (Fig. 3b). In contrast, the area located south of the SPI (GCN and CDI) showed decreases with values as low as -31% (Fig.

325   3b). These regional differences may be due to several factors, including improved outlines and corrections from local inventories and differences in acquisition dates (Fig. 3d). While 84.7% of the glacier area in RGI6 has an acquisition date in 2000, only 10.5% of the glacier area in RGI7 has an acquisition date in the same year (91.7% between 2000–2003, including both years).
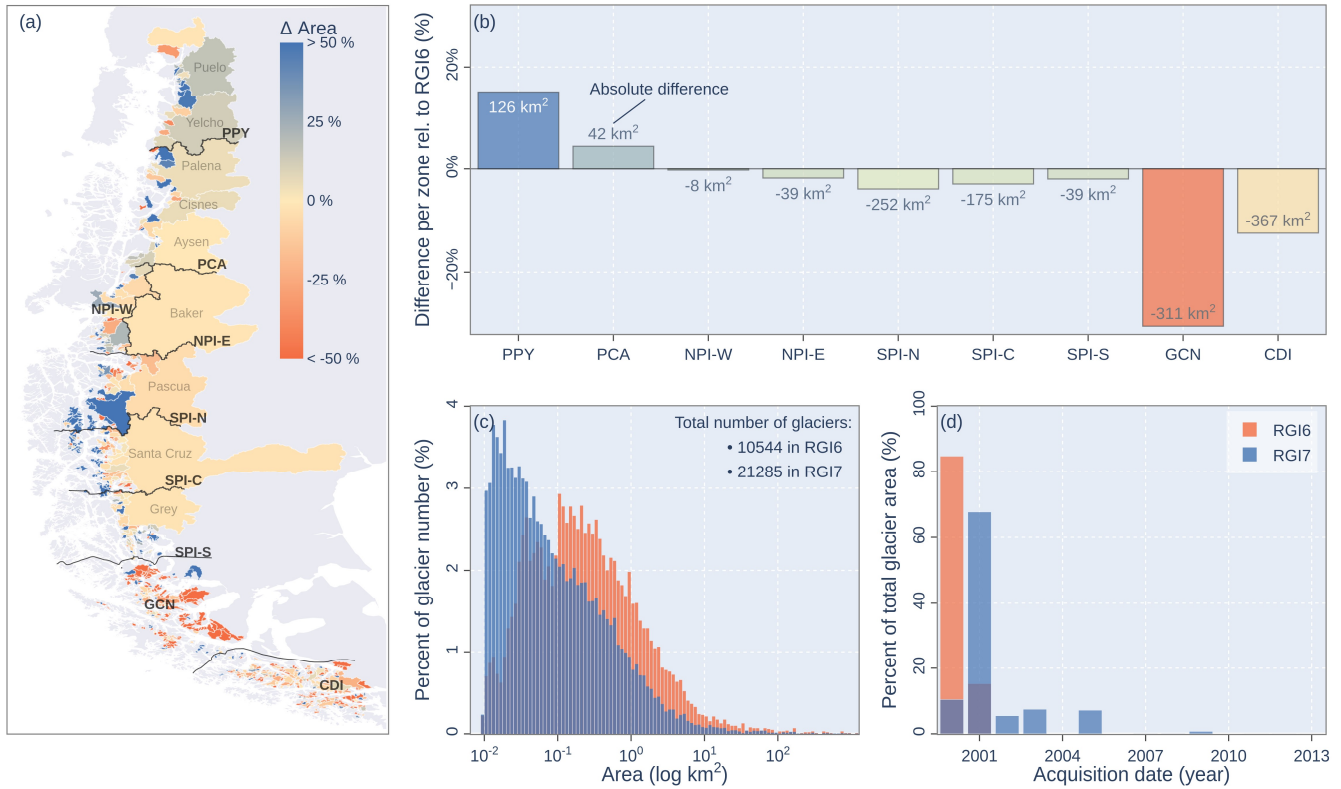
Figure 3. Comparison between Randolph Glacier Inventory (RGI) versions 6 and 7. Difference in area a) per catchment and b) per hydrological zone considering RGI6 as reference. The names in grey in (a) correspond to the names of the main catchments, while the solid black line corresponds to the division between the hydrological zones defined in Fig. 1. The text in b) indicates the absolute difference in area (RGI7 – RGI6). c) Distribution of glacier area. d) Percent of glacier area per year of acquisition.

Ice volume was another source of uncertainty analysed in this study (Fig. 4). According to the F19 dataset, the hydrological zones comprising the SPI have an ice volume of 3,526 km^3, representing 68.8% of the study area. Conversely, the PPY, PCA, GCN and CDI zones accounted for only 8.9% of the total ice volume. The 26.6% of the study domain had a normalized thickness (ice volume divided by catchment area) of less than 1.0 m (Fig. 4a). Based on RGI6, the M22 dataset showed more ice volume than the F19 dataset in 81.7% of the total glacier area (overall volume difference of 11.1%; Fig. 4b), mainly in the Patagonian Icefield (Fig. 4c). In this area, the NPI and SPI zones showed increases of 135 km^3 and 469 km^3 (relative to F19), respectively. Only the PCA and CDI zones showed the opposite change, where the M22 dataset shows a lower total ice volume (Fig. 4c).
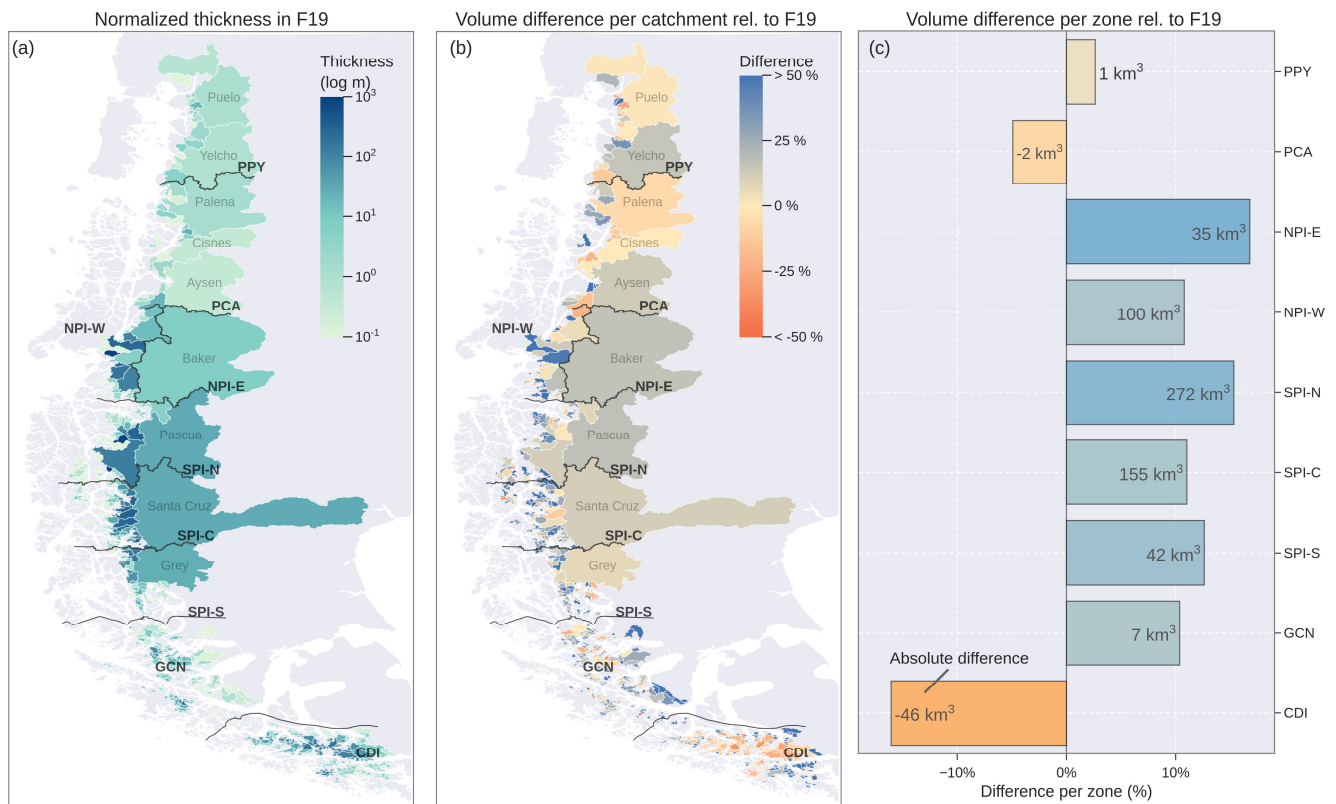
Figure 4. Volume comparison between Millan et al. (2022) (M22) and Farinotti et al. (2019) (F19) based on RGI6. a) Thickness normalized by the catchment area from F19 (in log scale). Percentage difference between M22 and F19 per b) catchment and c) hydrological zone considering F19 as reference. The grey names in (a) and (b) correspond to the names of the main catchments, while the solid black line corresponds to the division between the hydrological zones defined in Fig. 1. The text in c) indicates the absolute difference in volume (M22 - F19).

The historical climate of the glaciers of the southern Andes showed an important climatic diversity according to the PMET dataset, with an annual mean precipitation varying between 1,000 and 8,000 mm yr⁻¹ (Fig. 5a; 1980–2015). The spatial pattern of precipitation showed a clear difference between the western (> 4,000 mm yr⁻¹) and the eastern (< 2,000 mm yr⁻¹) side of the Andes (Fig. 5a). Mean precipitation was greater than 4,000 mm yr⁻¹ over 51.5% of the glacier area, and 95.0% of the glacier area showed a mean temperature above 0 ℃ (Fig. 5b). The four climate products used to model the historical evolution of the glaciers showed important differences in precipitation and temperature (Fig. 5c-e). In relation to PMET, ERA5 and MSWEP showed total differences in solid precipitation of 46.9% and -55.6% (glacier area weighted mean; Fig. 5c), respectively. The relative differences in temperature were mostly less than 1 ℃, except for ERA5, which showed a cold bias (Fig. 5d). These differences resulted in discrepancies of less than 25% for the positive degree-day sum (Fig. 5e).
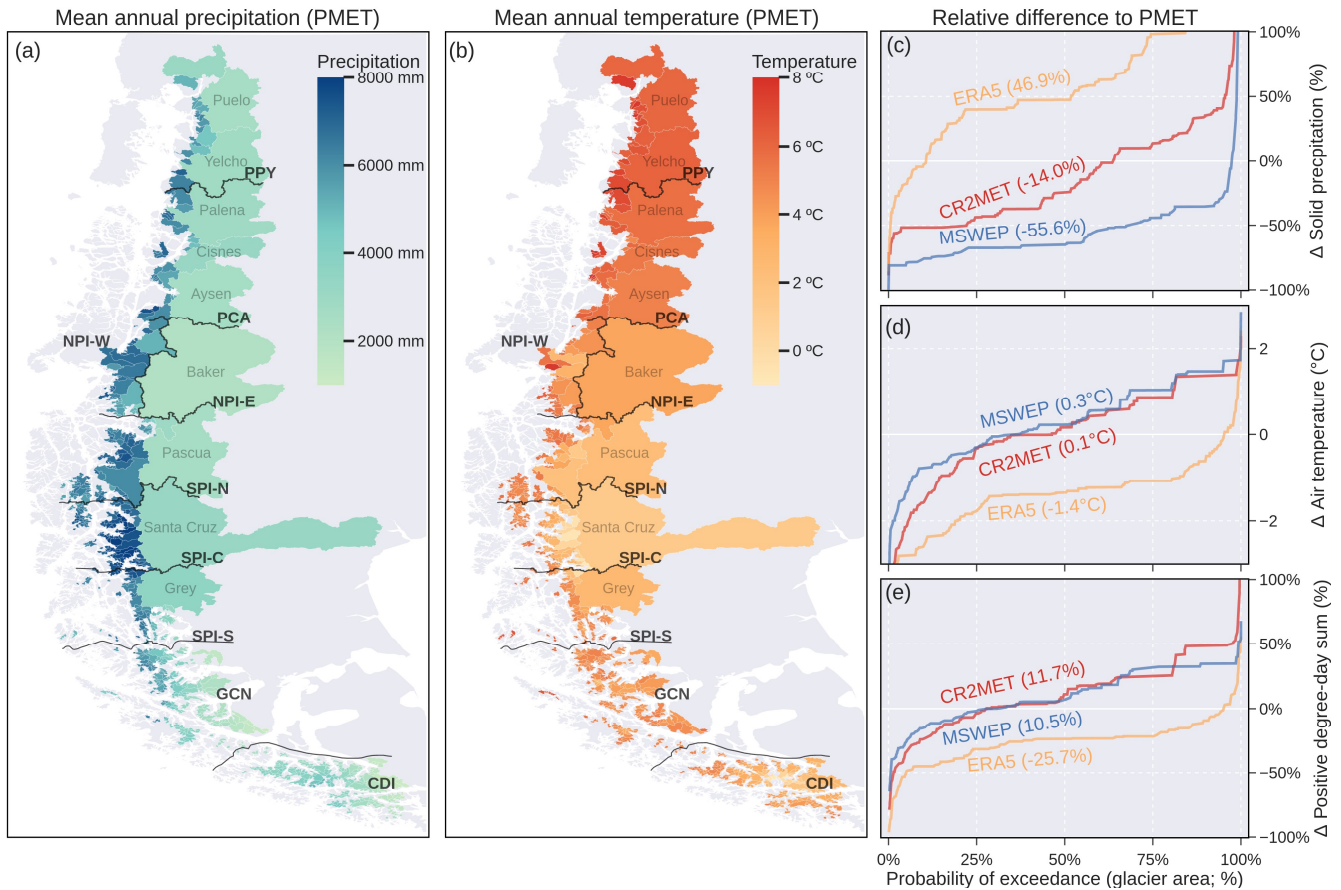
Figure 5. Historical reference climate in terms of annual precipitation (a) and temperature (b) according to the PMET dataset. Long-term averages (1980-2015) were calculated using only the glacierized grid cells of each catchment. The grey names in (a) and (b) correspond to the names of the main catchments, while the solid black line corresponds to the division between the hydrological zones defined in Fig. 1. Differences between PMET and CR2MET, ERA5 and MSWEP/MSWX sorted by glacier area for solid precipitation (c), temperature (d), and positive degree-day sum (e). The values in parenthesis indicate the glacier area weighted means.

4.1.2 Precipitation and temperature climate projections (2020–2099)

The climate projections for the end of the century (2070–2099) showed clear latitudinal patterns (Fig. 6a, b). Overall, the northern area was characterized by a warmer and drier future climate, while the southern area showed a slight increase in precipitation accompanied by a slight increase in temperature. The GCMs showed a high model agreement in all zones (> 80% of the models agree on the sign of the change), except in the SPI and GCN zones (Fig. 6a). The climate projections for the catchments varied according to the SSP scenario. Under the SSP1-2.6 scenario, the 54% of the glacier area is projected to experience a decline in precipitation (Fig. 6c). This percentage increases to 83% under the SSP5-8.5 scenario. For temperature, the glacier area weighted warming varies from 1.0 ºC in SSP1-2.6 to 2.7 ºC in SSP5-8.5 (Fig. 6d).
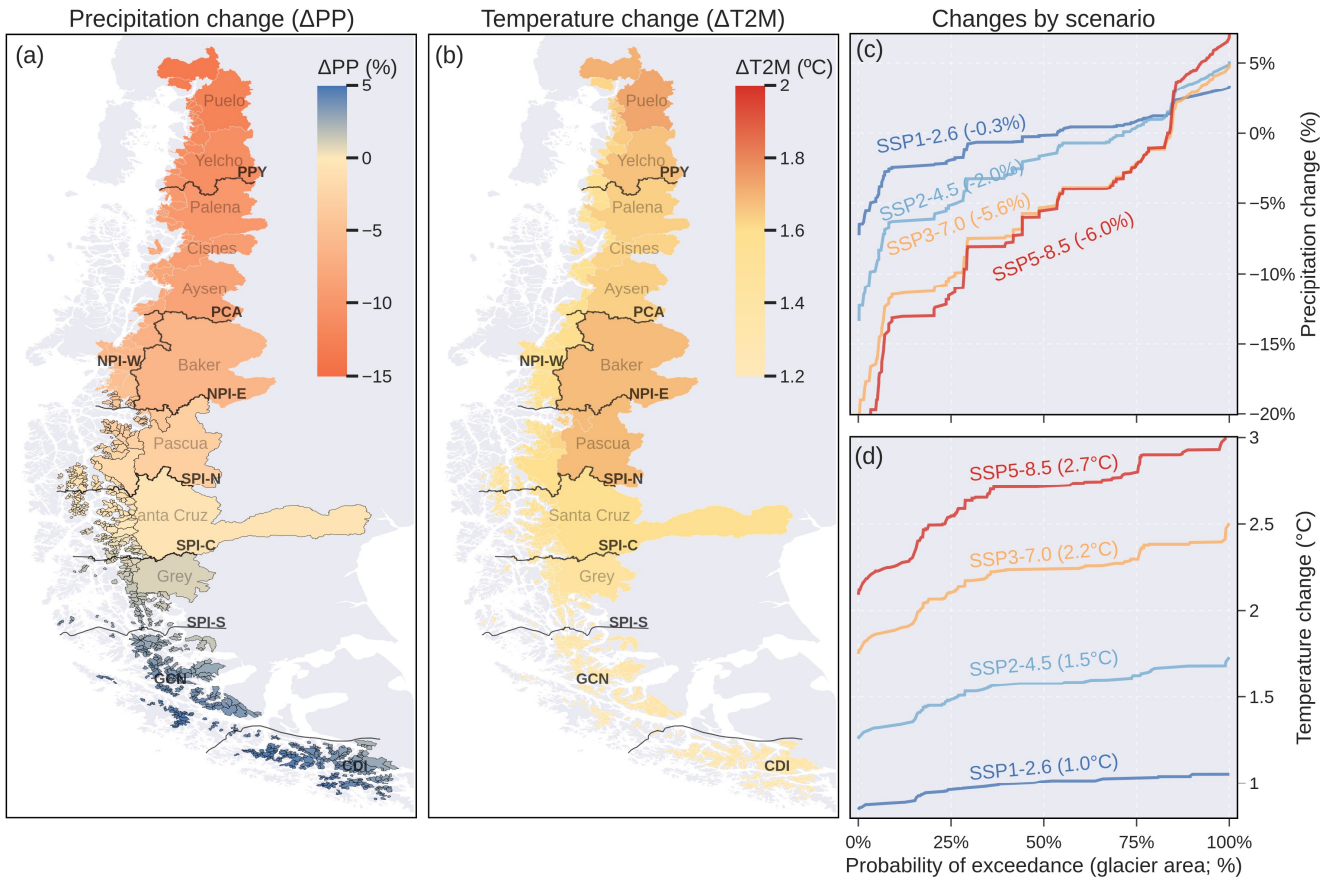
Figure 6. Multi-model means (n = 10) of future precipitation (a) and temperature change (b) considering the SSP 2-4.5 scenario (1980–2015 *vs.* 2070–2099). Means were calculated using only the glacierized grid cells of each catchment. The catchments with black outlines indicate low model agreement, where less than 80% of the models agree on the sign of the change. The grey names in (a) and (b) correspond to the names of the main catchments, while the solid black line indicates the division between the hydrological zones defined in Fig. 1. Differences by scenario for precipitation (c) and temperature (d). The values in parenthesis indicate the glacier area weighted means.

4.1.3 Combined uncertainty of future climate

Future climate uncertainty considered four reference climate products, ten General Circulation Models (GCMs), four different Shared Socioeconomic Pathways (SSPs), and three bias correction methods (MVA, QDM, and MBCn), resulting in 480 possible combinations (Fig. 7). The standard deviation of the mean annual precipitation in the long term (2070–2099) was greater than 1,000 mm in 68% of the glacier area (Fig. 7a). Similarly, the standard deviation of the temperature was greater than 1.0 °C in 89% of the glacier area (Fig. 7b). The precipitation showed a greater variability (expressed as coefficient of variation) in the glaciers located on the western side of the Southern Andes (Fig. 7a). On the other hand, the greater variability of temperature was concentrated in the SPI-C and CDI zones (Fig. 7b). For all variables, the reference climate was the most important source of uncertainty (Fig. 7c-e). The difference between SSPs and GCMs was more pronounced for temperature

and positive degree-day sum (Fig. 7d,e) than for solid precipitation (Fig. 7c). The different bias correction methods (BCM) converged to similar values with no important differences between them.
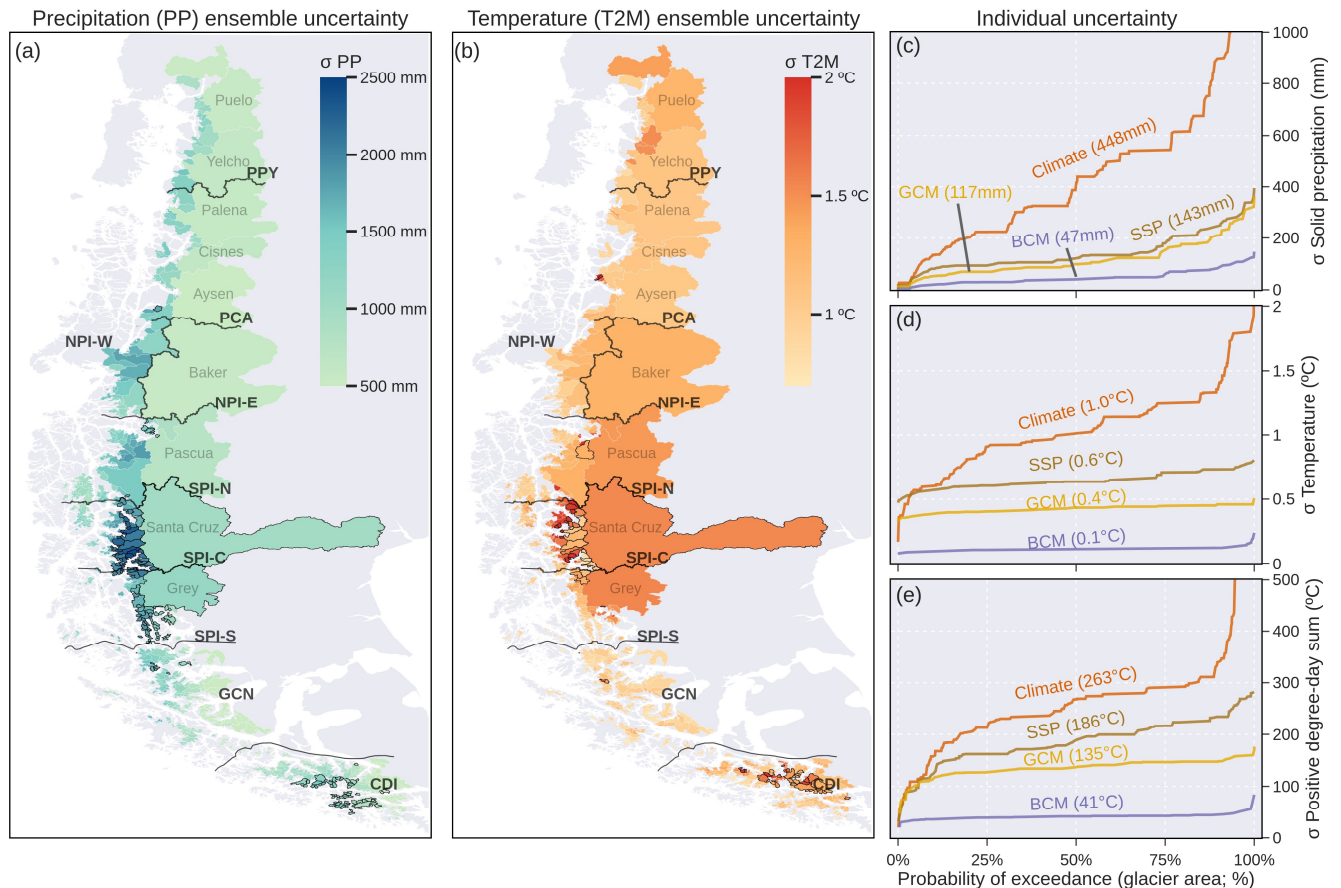
Figure 7. Future climate uncertainty (standard deviation; σ) in mean annual precipitation (a) and temperature (b) obtained from the complete ensemble (2070–2099). The catchments with a coefficient of variation greater than 40% have black outlines. Means were calculated using only the glacierized grid cells of each catchment. The grey names in (a) and (b) correspond to the names of the main catchments, while the solid black line indicates the division between the hydrological zones defined in Fig. 1. Individual uncertainty (in terms of glacier area) in solid precipitation (c), temperature (d) and positive degree-day sum (e) across different reference climates, emission scenarios (SSPs), general circulation models (GCMs) and bias correction methods (BCM). The values in parenthesis indicate the glacier area weighted means.

4.2 Glacio-hydrological projections

Projections from OGGM indicate that the glacier volume loss of recent decades will continue (Fig. 8). Considering the full set of SSP scenarios (n = 1920), 68% ± 21% (mean ± one standard deviation) of the total glacier area will lose more than 50% of their current (year 2020) volume by the end of the century (Fig. 8a). The results suggest that ice loss will vary according to different sources of uncertainty. Considering the prolongation of historical climate conditions, 24% ± 6% of the total glacier

ice is committed to melt in the long term (year 2099 in Fig. 8b). Aggregating the time series by emission scenario (n = 480 per SSP), the volume loss varied from 46 ± 9% in SSP1-2.6 to 67 ± 11% in SSP5-8.5, with clear spatial differences (Fig. 8c-f). In the northern region (PPY and PCA), the projected loss is exacerbated by the low ice volume (Fig. 4) and precipitation projections (Fig. 5), resulting in percentage losses exceeding 70% under all scenarios (Fig. 8c). Under the high emissions scenario (SSP 5-8.5), the percentage loss in NPI, SPI and the southern area (GCN and CDI) is projected to be 64% ± 8%, 68% ± 12% and 71% ± 7%, respectively (Fig. 8d-f). At the hydrological zone scale (Fig. S1), the confidence intervals for volume and area in the reference period are consistent with the differences found between the glacier inventories (Fig. 3) and ice thickness datasets (Fig. 4). Similar to the ice volume projections, the mean specific mass balance diverges strongly depending on the emission scenarios (Fig. S1).
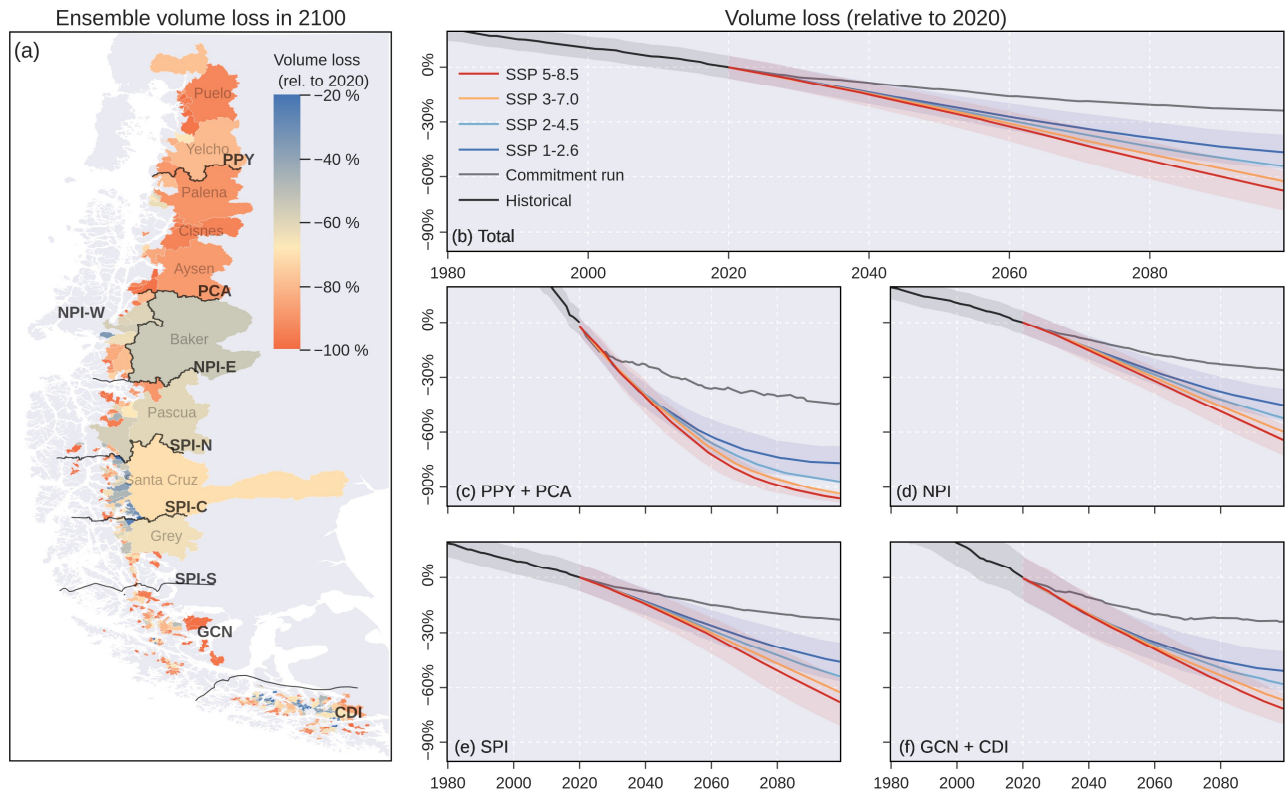
Figure 8. Glacier volume loss relative to 2020. a) Mean volume loss in 2100 derived from the full ensemble (n = 1920). Volume loss for the sum of all catchments (b), the northern area including PPY and PCA (c), the Northern Patagonian Icefield (d), the Southern Patagonian Icefield (e) and the southern area including GCN and CDI (f). The solid line represents the mean for each scenario, while the uncertainty bands represent ± one standard deviation (shown only for historical, SSP 1-2.6 and SSP 5-8.5 for visualization purposes). Volume, area and specific mass balance by hydrological zone are shown in Fig. S1. The commitment run considers a pseudo-random climate based on the period 1985–2015.

The volume loss drives changes in the hydrological contribution of glaciers in the Patagonian Andes (Fig. 9). Considering the full set of SSP scenarios (n = 1920), 34% ± 13% of the glacier area has already peaked in terms of glacier melt (year 2020; Fig. 9a). The total glacier melt for the study domain in the reference period (1980–2015) was 2,051 ± 537 m³ s⁻¹ (Fig. 9b). For this total, the northern area (PPY and PCA), NPI, SPI and the southern area (CGN and CDI) contributed with 4.6%, 20.5%, 66.0% and 8.8% (Fig. 9c-f), respectively. The projected trajectories of glacier melt varied slightly among emissions scenarios (n = 480 per SSP), and the projections and their uncertainties tended to converge towards the end of the century (Fig. 9b). For example, the mean glacier melt in 2070–2099 varies from 1,555 ± 372 m³ s⁻¹ in SSP 1-2.6 to 1,784 ± 369 m³ s⁻¹ in SSP 5-8.5 for the whole region. While most hydrological zones are projected to experience a steady decrease in glacier melt, the SPI zones show slightly diverging trajectories in their mid-century meltwater contribution depending on the emission scenario (Fig. 9e). To the south of SPI, the slight increase in precipitation projections (Fig. 6) buffers the decrease in glacier melt, maintaining the contribution of glacier runoff. In all hydrological zones, the ratio between glacier runoff and melt is close to 60% in the reference period, and decreases to 40% towards the end of the century (Fig. S2).

Figure 9. Glacier melt projections for the Patagonian Andes. a) Peak water year obtained from the complete ensemble (n = 1920). Glacier melt evolution for the sum of all catchments (b), the northern area including PPY and PCA (c), the Northern Patagonian Icefield (d), the Southern Patagonian Icefield (e) and the southern area including GCN and CDI (f). The solid line represents the

4.3 Influence on glacio-hydrological signature

The glacio-hydrological signature was represented by ten metrics that characterize the hydrological regime of each catchment (Table 1). Regardless of the variable (glacier runoff or melt), the permutation feature importance of RF models showed that the differences between the historical reference climates contributed most to the total uncertainty (Fig. 10). This was especially clear for the reference magnitude, peak water magnitude, inter-annual variability and reference seasonal contribution and variability metrics, where the reference climate accumulated more than 50% of the total RMSE loss after the permutations. Considering glacier melt only, the accumulated RMSE loss of the historical sources of uncertainty (glacier inventory, glacier volume, and reference climate) was greater than that of the future sources (GCM, SSP, and BCM) in eight signatures (only five for glacier runoff), including the peak water metrics. In the long-term (trend and change signatures), the historical sources accumulated a RMSE loss similar to that of the future sources. In these cases, the selection of reference climate or GCM was as important as the emission scenario (SSP). The selection of glacier inventory was more important than the ice thickness dataset for most metrics, while the importance of the bias correction method (BCM) was significant (median > 10%) only for the reference seasonal shift (Fig. 10). Consistently, the relative importance of future sources was 0% for all metrics calculated from the reference period (Table 1).

No clear spatial patterns were detected in the main source of uncertainty (i.e., the variable that accumulated most RMSE loss; Fig. S3 and S4). Considering the glacier melt signatures (Fig. S3), the future sources of uncertainty were the main source in only 17% ± 21% (mean ± one standard deviation) of the total glacier area. In contrast, the reference climate was the main source of uncertainty in 69% ± 22% of the glacier area. In comparison to the glacier runoff signatures, the importance of the reference climate decreases to 58% ± 31% of the glacier area (Fig. S4).
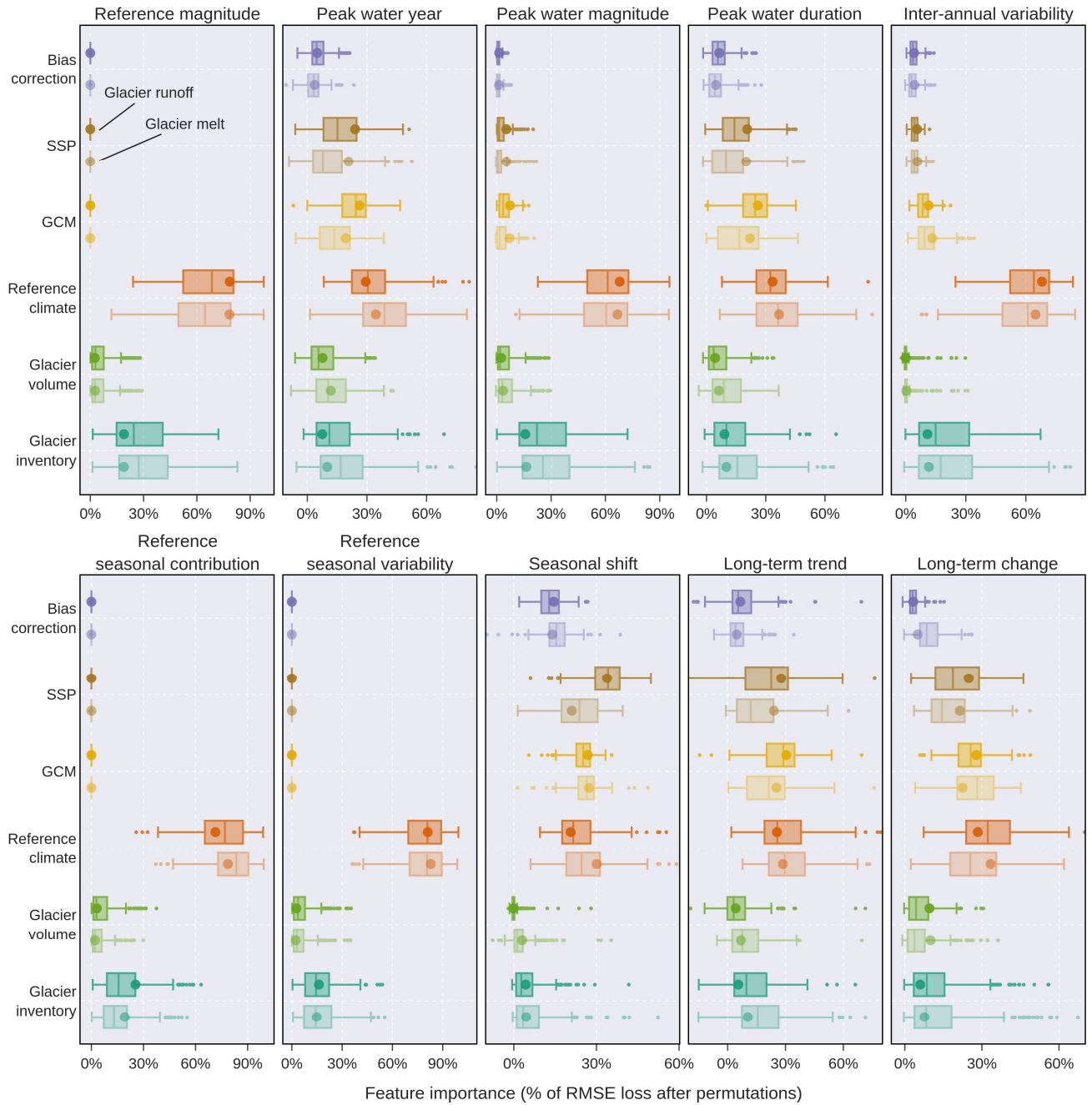
Figure 10. Importance of each source of uncertainty for the glacio-hydrological signatures obtained from the glacier runoff (dark
465 **colours) and melt (light colours). The importance of each source on the glacio-hydrological signatures (Table 2) is represented as the**
percentage of the average change in the Root Mean Square Error (RMSE), with high values indicating a greater importance. The
circles correspond to the glacier area weighted means. Note that each panel has a different range.

5 Discussion

5.1 Hydrological response of Patagonian glaciers to climate change

470 The primary objective of glacio-hydrological modelling studies has been to assess the future impacts of climate change (Van Tiel et al., 2020), and therefore GCM and SSP choices have commonly been part of the uncertainty analysis of previous modelling efforts. For the first time, this study incorporated four additional sources of uncertainty (both historical and future) to generate 1,920 possible future evolution scenarios in the Patagonian Andes.

As expected, volume loss showed a strong dependence on the emission scenario with total projected losses ranging from 48 ± 475 9% in SSP1-2.6 to 69 ± 10% in SSP5-8.5 (Fig. 8b). Despite the dependence of the specific mass balance (units: kg m^{-2} yr^{-1}) on the emission scenarios (Fig. S1), the ice melt component of runoff (units: m^3 s^{-1}) did not show a clear dependence on the emission scenario (Fig. 9), as it is not normalized by glacier area, which decreases during the century (Fig. S1). Only a few hydrological zones showed clear differences in their mid-century meltwater contribution between SSP scenarios, such as NPI-W and SPI-N. This is partly explained by the fact that 30% ± 13% of the glacier area has already peaked in terms of glacier 480 melt (year 2020; Fig. 9a). The uncertainty in the glacier melt component is lower than that of total glacier runoff (Fig. S2), because the latter also entails the liquid precipitation and off-glacier snowmelt components, which are determined more by the reference climate than by model parameters (Fig. 7).

Although glacio-hydrological studies are scarce in the Patagonian Andes, the Baker River Basin (NPI-E in Fig. 1; 7.2% of glacier area) provides a point of comparison with previous studies. Our study revealed a slight increase in glacier runoff (3% 485 per decade) between 1980 and 2015. This finding is consistent with previous studies by Dussaillant et al. (2019), who observed a similar trend from 2001 to 2017 using ASTER stereo images and stream gauges, and Caro et al. (2024) who reported a 10% increase in glacier melt from 2000 to 2019 using the OGGM model (Table S1). In a longer time frame, Huss and Hock (2018) found that the peak water of the Baker River has already occurred or will occur in the coming years regardless of the emission scenario (2015 ± 18 and 2020 ± 16 for RCP 2.6 and RCP 8.5, respectively), which is in agreement with our results indicating 490 that the glacier runoff may have peaked (2021 ± 15) considering all scenarios.

5.2 Hydrological importance of data uncertainty

All 10 glacio-hydrological metrics across the catchments show a considerable uncertainty to modelling choices (Fig. 10). Previous studies have shown that accurate estimates of glacier outlines (Li et al., 2022) and initial ice volumes (Gabbi et al., 2012) have played a pivotal role in ensuring reliable projections of volume and runoff. In our study, despite the larger relative 495 differences in glacier volume than in glacier area (11.1% vs. 4.0% of overall difference; Fig. 3 and 4), the selection of glacier inventory was more important for most glacio-hydrological metrics (Fig. 10). The importance of these glacier attributes was only superseded by the choice of the climate in the historical period (Fig. 10). Our uncertainty analysis showed that the

reference climate was the most important source in 69% ± 22% of the glacier area for glacier melt (Fig. S3) and 58% ± 31% of the glacier area for glacier runoff (Fig. S4). The importance of the reference climate is that it establishes baseline conditions against which future changes can be assessed. Its influence on temperature and precipitation directly shapes the seasonal response of glaciers, affecting both melting and accumulation processes. Finally, the reference climate will also influence the parameter calibration (see below) and therefore the model sensitivity to climate change.

Despite the large variability in climate, geography and glacier characteristics in the Patagonian Andes, only a few regions showed a low sensitivity to the reference climate. This is partly explained by the fact that some climate products showed overall relative differences of almost 50% in solid precipitation (Fig. 5), which dominates glacier runoff and melt evolution. For the long-term trend of glacier melt (Fig. S3), the GCMs and SSPs were the main source of uncertainty in the Patagonian Icefields (SPI, NPI and CDI), areas characterised by mostly neutral precipitation projections (Fig. 6) and the presence of high ice volumes (Fig. 4). The greater importance of the GCMs and SSPs was also observed in the northern area (PPY and PCA) for the long-term change in glacier melt. When considering glacier runoff (Fig. S4), which includes liquid precipitation as glaciers retreat, the importance of the SSP scenario increases in several metrics, such as seasonal shift and long-term change.

5.3 Influence of model calibration

The calibration of large-scale glacier model parameters is usually glacier-specific and varies according to the glacier model and the available data (for an extensive overview, refer to Zekollari et al. 2022). For example, in the Global Glacier Evolution Model (GloGEM; Huss and Hock, 2015), the calibration follows a sequential approach where glaciological observations are matched by adjusting a precipitation factor, then a melt factor and finally a temperature bias parameter within predefined ranges. This type of procedure strongly adjusts the forcing climate data to match the expected values from the combination of a mass balance model and observations, which likely explains why Compagno et al. (2021) found that the choice of the reference climate leads to differences of only 7% in the remaining ice volume by 2100 in Scandinavia and Iceland. However, in High Mountain Asia and using another methodology, Watanabe et al. (2019) found that the differences between the reference climate introduced uncertainties of about 15% into projected changes in glacier volume.

Considering the scaling effect of the precipitation factor on glacier runoff (Schuster et al., 2023), our study, in turn, chooses not to correct the historical climate dataset (i.e., maintaining $P_f = 1$), and therefore the historical climate uncertainty is incorporated into the model calibration and then into the projections. This approach recognises the inherent variability in precipitation estimates and aims to capture the range of potential 'true' precipitation values. In particular, certain regional climate datasets used in our analysis, such as PMET and CR2MET, are already subject to bias correction procedures to address potential underestimation of precipitation in high mountain areas. Thus, by incorporating historical climate uncertainty, our

methodology aims to provide a robust framework for glacier runoff projections. Alternatively, future studies could use ensemble meteorological datasets (e.g., Tang et al. 2022) to incorporate uncertainty into their assessments.

In recent years, the calibration workflow of large-scale glacier models has evolved to incorporate model parameter uncertainty as a significant source of uncertainty. For example, the Python Glacier Evolution Model (PyGEM) uses Bayesian inference to calibrate the three parameters of for each glacier based on Markov Chain Monte Carlo (MCMC) methods (Rounce et al., 2020, 2023). Interestingly, when comparing the mean projected volume loss disaggregated by hydrological zone and SSP scenario with Rounce et al. (2023) projections, the difference with our study was only 4.4% (RMSE; Fig. S5). This suggests a remarkable consistency in projected glacier evolution despite potential differences in the sources of uncertainty considered between the studies.

5.4 Limitations and potential implications

There are several sources of uncertainty that were not considered in this study, such as downscaling strategies (e.g., temperature lapse rates), observation uncertainty, the use of frontal ablation parameterisation schemes, the surface mass balance model (e.g., degree-day *vs.* energy balance), and the ice-flow model itself. These are acknowledged shortcomings of our study and should be further investigated. For example, Schuster et al. (2023) using the OGGM model showed that the use of spatially and seasonally variable lapse rates has the most systematic influence on glacier projections with smaller glacier volumes by the end of the century compared to the constant option. The geodetic mass balance used in the dynamic calibration process is another source of uncertainty. While Hugonnet et al. (2021) obtained a specific mass balance of -720 ± 70 kg m^{-2} yr^{-1} for the complete RGI region (2000–2019), Braun et al. (2019) and Dussaillant et al. (2019) estimated values of -640 ± 20 kg m^{-2} yr^{-1} (2000–2015) and -720 ± 220 kg m^{-2} yr^{-1} (2000–2018), respectively. Minowa et al. (2021) estimated that frontal ablation was -24.1 ± 1.7 Gt a^{-1} (2000–2019), representing $34 \pm 6\%$ of total ablation. The study of calving glaciers adds a layer of complexity, as additional processes require potential parameterisations and adjustments, which are also subject to uncertainty (Van Tiel et al., 2020). Using the OGGM model, Malles et al. (2023) found that the global mean sea level rise contribution at the end of this century is reduced by ~9% when marine frontal processes were considered in Northern Hemisphere glaciers. Surface mass balance models can also play an important role in glacier evolution, but the lack of data hinders the assessment of the added value of more model complexity (e.g., Temme et al., 2023; Schuster et al., 2023; Huss and Hock, 2015).

The use of ground-based observations can help to reduce the overall uncertainty. For example, the use of observations of ice thickness, such as those based on ground-penetrating radar or airborne surveys, can help to select a better dataset for the study area. However, these observations are spatially and temporally scarce in the Patagonian Andes (e.g., Millan et al., 2019). Furthermore, the generation of large-scale ice thickness datasets requires the compilation of numerous datasets derived from different acquisition dates which hinders regional validation (Hock et al., 2023). The reference climate can also be assessed

using ground-based data. However, the current scarcity, poor quality control protocols, and lack of continuity and reliability of meteorological stations is a very important limitation to properly understand atmospheric processes at high elevations (Condom et al., 2020; Masiokas et al., 2020). Recent studies have attempted to narrow the ranges of uncertainty using, for example, regional estimates of moisture flux (Sauter, 2020) and catchment hydrological balance (Aguayo et al., 2024). Future sources of uncertainty could potentially be reduced using a GCM screening approach. Using Chile as a case study, Gateño et al. (2024) recently proposed an approach that goes beyond bias-related metrics to include metrics related to the ability of GCMs to reproduce teleconnection responses that can affect regional climate variability and trends. Out of the 10 selected GCMs in our study, four are included in the screening recommendation of Gateño et al. (2024) (more details in Table S2).

The implications of our study extend far beyond the Patagonian Andes and resonate with global concerns about the effects of climate change on the hydrological cycle in high mountain regions. These regions very often face challenges in constraining climate estimates due to a low density of meteorological stations (e.g., Beck et al., 2020). These limitations have led to substantial modelling uncertainties in the hydrological cycle (Tang et al., 2023), which can be projected into the future in climate change impact studies (Tarek et al., 2021). Our study is the first to assess the influence of the reference climate on evolution of glacier runoff, resulting in differences from previous studies (Fig. 10). In the Southern Andes, the Glacier Model Intercomparison Project Phase 2 (GlacierMIP2) showed that the uncertainty in the emission scenario is the largest source for the specific mass balance rate (Marzeion et al., 2020). Similarly, Mackay et al. (2019) found that the emission scenarios were also the dominant source for projections of streamflow during the melt season in Iceland, contributing up to 65% of the total projected uncertainty. In our study, the relatively greater influence of the future sources was limited to the long-term metrics, where the selection of the emission scenario or the GCM was as important as the reference climate (Fig. 10). This underscores that future glacio-hydrological projections are strongly shaped by modellers' choices, which should be guided by a systematic review of local datasets to adequately justify modelling choices. In addition, further research into the mechanisms driving the observed differences in precipitation and temperature, and their implications for glacier runoff dynamics, could provide valuable insights into the broader hydrological response of glaciated regions to changing climate conditions.

6 Conclusions

In this study, we investigated the importance of six sources of data uncertainty in ten glacio-hydrological signatures covering the necessary categories to characterize the glacio-hydrological regime of each catchment. For this purpose, we used the Open Global Glacier Model (OGGM) to project the potential change in the hydrological contribution of each glacier (area > 1km^2; 2,034 glaciers in RGI6) in the Patagonian Andes (40–56° S) under 1920 potential scenarios. Based on these projections, we used the permutation importance of random forest regression models to calculate the relative importance of each source of data uncertainty. Our main findings are as follows:

- The sources of data uncertainty showed relative differences of varying magnitude. The importance of the selection of glacier inventory and ice thickness source was masked by the reference climate. While the glacier inventory and ice thickness source showed overall differences close to 10%, the different climate alternatives showed differences of more than 50% for solid precipitation, for example. Among all contributors to future climate uncertainty (2070–2099), the reference climate was also the most important source for all variables, followed by the SSP, the GCM, and finally the bias correction method used.

- The volume loss of glaciers varies significantly with emission scenarios, ranging from 46 ± 9% in SSP1-2.6 to 67 ± 11% in SSP5-8.5. However, while the specific mass balance is influenced by emission scenarios, glacier melt doesn't show a clear dependence due to changes in glacier area over time. Uncertainty in glacier melt is reduced compared to glacier runoff due to the smaller influence of the reference climate, which mainly influences glacier runoff through past climate-dependent liquid precipitation.

- For eight glacio-hydrological signatures obtained from the glacier melt evolution, the uncertainty from historical sources exceeded that from future sources, underscoring the critical role of modeler decisions during the calibration process. Considering all glacier melt signatures, the reference climate was the main source of uncertainty in 69% ± 22% of the glacier area. For long-term metrics (trend and change), factors not typically considered in regional studies, such as the selection of GCMs and reference climate, were as important as emission scenarios.

Our results shed light on the evolution of glacier runoff in the Patagonian Andes and provide new insights into the impacts of data uncertainty. To our knowledge, the present study is the first large-scale assessment of the impact of multiple sources of data uncertainty (both historical and future) from a perspective beyond future glacier volume loss. In order to advance with adaptation plans for the long-term sustainability of local ecosystems, future studies should address sources of uncertainty not considered in this study (e.g., parameterization of frontal ablation, climate downscaling and surface mass balance and ice-flow models), and extend the scope from glaciers to downstream hydrology. Downstream hydrology can play a critical role in the seasonal and interannual water release during dry seasons (Drenkhan et al., 2022), attenuating the consequences of glacier shrinkage (e.g., Somers et al., 2019). Finally, we hope that our rigorous uncertainty quantification helps to prioritize future efforts (e.g., reference climate) to reduce glacio-hydrological modelling gaps in the Patagonian Andes.

Appendix A: dynamic calibration minimization algorithm

At the beginning, a first guess of the control variable (T_{spinup} or μ^*) is used and evaluated. If the mismatch between model and observation happens to be close enough, the algorithm stops. Otherwise, the second guess depends on the calculated first guess mismatch. For example, if the first resulting area is smaller (larger) than the searched one, the second temperature bias will be colder (warmer). This is because a colder (warmer) temperature leads to a larger (smaller) initial glacier state. The same idea

is used for matching the geodetic mass balance. If the second guess is still unsuccessful, the previous value pairs (control variable, mismatch) are used for all subsequent guesses to determine the next guess. This is done by fitting a stepwise linear function to these pairs and then setting the mismatch to 0 to obtain the next guess (this method is similar to the one described in Appendix A of Zekollari et al. 2019).

620 **Code availability**

The complete code repository can be found at: https://github.com/rodaguayo/glacier_uncertainties

Data availability

The glacier outlines from RGI6 and RGI7 were downloaded from https://nsidc.org/data/nsidc-0770/versions/6 (last access: May 16, 2024) and https://nsidc.org/data/nsidc-0770/versions/7 (last access: May 16, 2024), respectively. NASADEM was 625 downloaded from: https://lpdaac.usgs.gov/products/nasadem_hgtv001 (last access: May 16, 2024). Ice thicknesses datasets from Millan et al. (2022) and Farinotti et al. (2019) were downloaded from https://doi.org/10.6096/1007 (last access: September 28, 2024) and https://doi.org/10.3929/ethz-b-000315707 (last access: May 16, 2024), respectively. PMET v1.0 was downloaded from https://doi.org/10.5281/zenodo.7992761 (last access: May 16, 2023). CR2MET v2.5 was downloaded from https://doi.org/10.5281/zenodo.7529682 (last access: May 16, 2024). ERA5 was downloaded from 630 https://cds.climate.copernicus.eu/#!/home (last access: May 16, 2024). MSWEP v2.8 was downloaded from https://www.gloh2o.org/mswep/ (last access: May 16, 2024). CMIP6 data was downloaded from the Google cloud storage provided by the Pangeo initiative (https://storage.googleapis.com/cmip6/pangeo-cmip6.json, last access: May 16, 2024). The complete set of results provided in this study is available at: https://doi.org/10.5281/zenodo.11353065

Author contributions

635 This study was conceived and designed by RA, FM and LS. RA collected the data and performed the modelling and core data analysis. PS implemented and developed the dynamic calibration algorithm. MS, AC, JL, MA, JM, and LU contributed to the analysis and discussion of the results and drafting of the manuscript. All authors revised the manuscript, provided feedback, and contributed to the preparation of the figures and tables. All authors approved the final version of the manuscript.

Acknowledgements

640 RA would like to acknowledge the support of the Open Global Glacier Model (OGGM) community for their valuable assistance, collaboration, and commitment to open science. JM publishes with the permission of the executive director, British Geological Survey (UKRI).

Financial support

RA was supported by the National Agency for Research and Development (ANID) PFCHA/DOCTORADO
645 NACIONAL/2019 – 21190544 and by the European Research Council (ERC) under the European Union's Horizon Framework research and innovation programme (grant agreement N°101115565; ICE^3 project). LS's contribution was funded by her DOC Fellowship of the Austrian Academy of Sciences at the Department of Atmospheric and Cryospheric Sciences, University of Innsbruck (No. 25928). LS's, PS's and FM's contributions were funded from the European Union's Horizon 2020 research and innovation programme under grant agreement No. 101003687. This text reflects only the author's view, and that the Agency
650 is not responsible for any use that may be made of the information it contains. JM's contribution was funded by the Natural Environment Research Council (NERC) MCNC Grant TerraFirma NE/W004895/1.

References

Aguayo, R., León-Muñoz, J., Aguayo, M., Baez-Villanueva, O. M., Zambrano-Bigiarini, M., Fernández, A., and Jacques-Coper, M.: PatagoniaMet: A multi-source hydrometeorological dataset for Western Patagonia, Sci Data, 11, 6,
655 https://doi.org/10.1038/s41597-023-02828-2, 2024.

Ayala, Á., Farías-Barahona, D., Huss, M., Pellicciotti, F., McPhee, J., and Farinotti, D.: Glacier runoff variations since 1955 in the Maipo River basin, in the semiarid Andes of central Chile, The Cryosphere, 14, 2005–2027, https://doi.org/10.5194/tc-14-2005-2020, 2020.

Barcaza, G., Nussbaumer, S. U., Tapia, G., Valdés, J., García, J.-L., Videla, Y., Albornoz, A., and Arias, V.: Glacier inventory
660 and recent glacier variations in the Andes of Chile, South America, Annals of Glaciology, 58, 166–180, https://doi.org/10.1017/aog.2017.28, 2017.

Beck, H. E., Wood, E. F., Pan, M., Fisher, C. K., Miralles, D. G., van Dijk, A. I. J. M., McVicar, T. R., and Adler, R. F.: MSWEP V2 Global 3-Hourly 0.1° Precipitation: Methodology and Quantitative Assessment, Bulletin of the American Meteorological Society, 100, 473–500, https://doi.org/10.1175/BAMS-D-17-0138.1, 2019.

665 Beck, H. E., Wood, E. F., McVicar, T. R., Zambrano-Bigiarini, M., Alvarez-Garreton, C., Baez-Villanueva, O. M., Sheffield, J., and Karger, D. N.: Bias correction of global high-resolution precipitation climatologies using streamflow observations from 9372 catchments, Journal of Climate, 33, 1299–1315, https://doi.org/10.1175/JCLI-D-19-0332.1, 2020.

Beck, H. E., Dijk, A. I. J. M. van, Larraondo, P. R., McVicar, T. R., Pan, M., Dutra, E., and Miralles, D. G.: MSWX: Global 3-Hourly 0.1° Bias-Corrected Meteorological Data Including Near-Real-Time Updates and Forecast Ensembles, Bulletin of the American Meteorological Society, 103, E710–E732, https://doi.org/10.1175/BAMS-D-21-0145.1, 2022.

670

Bennett, K. E., Miller, G., Busey, R., Chen, M., Lathrop, E. R., Dann, J. B., Nutt, M., Crumley, R., Dillard, S. L., Dafflon, B., Kumar, J., Bolton, W. R., Wilson, C. J., Iversen, C. M., and Wullschleger, S. D.: Spatial patterns of snow distribution in the sub-Arctic, The Cryosphere, 16, 3269–3293, https://doi.org/10.5194/tc-16-3269-2022, 2022.

Boisier, J. P.: CR2MET: A high-resolution precipitation and temperature dataset for the period 1960-2021 in continental Chile., https://doi.org/10.5281/zenodo.7529682, 2023.

675

Braun, M. H., Malz, P., Sommer, C., Farías-Barahona, D., Sauter, T., Casassa, G., Soruco, A., Skvarca, P., and Seehaus, T. C.: Constraining glacier elevation and mass changes in South America, Nature Climate Change, 9, 130–136, https://doi.org/10.1038/s41558-018-0375-7, 2019.

Bravo, C., Quincey, D. J., Ross, A. N., Rivera, A., Brock, B., Miles, E., and Silva, A.: Air Temperature Characteristics, Distribution, and Impact on Modeled Ablation for the South Patagonia Icefield, Journal of Geophysical Research: Atmospheres, 124, 907–925, https://doi.org/10.1029/2018JD028857, 2019a.

680

Bravo, C., Bozkurt, D., Gonzalez-Reyes, Á., Quincey, D. J., Ross, A. N., Farías-Barahona, D., and Rojas, M.: Assessing Snow Accumulation Patterns and Changes on the Patagonian Icefields, Frontiers in Environmental Science, 7, 1–18, https://doi.org/10.3389/fenvs.2019.00030, 2019b.

685   Breiman, L.: Random Forests, Machine Learning, 45, 5–32, https://doi.org/10.1023/A:1010933404324, 2001.

Cannon, A. J.: Multivariate quantile mapping bias correction: an N-dimensional probability density function transform for climate model simulations of multiple variables, Climate Dynamics, 50, 31–49, https://doi.org/10.1007/s00382-017-3580-6, 2018.

Cannon, A. J., Sobie, S. R., and Murdock, T. Q.: Bias correction of GCM precipitation by quantile mapping: How well do methods preserve changes in quantiles and extremes?, Journal of Climate, 28, 6938–6959, https://doi.org/10.1175/JCLI-D-14-00754.1, 2015.

690

Caro, A., Condom, T., and Rabatel, A.: Climatic and Morphometric Explanatory Variables of Glacier Changes in the Andes (8–55°S): New Insights From Machine Learning Approaches, Front. Earth Sci., 9, 713011, https://doi.org/10.3389/feart.2021.713011, 2021.

695   Caro, A., Condom, T., Rabatel, A., Champollion, N., García, N., and Saavedra, F.: Hydrological response of Andean catchments to recent glacier mass loss, The Cryosphere, 18, 2487–2507, https://doi.org/10.5194/tc-18-2487-2024, 2024.

Cauvy-Fraunié, S. and Dangles, O.: A global synthesis of biodiversity responses to glacier retreat, Nat Ecol Evol, 3, 1675–1685, https://doi.org/10.1038/s41559-019-1042-8, 2019.

Chen, J., Brissette, F. P., and Leconte, R.: Uncertainty of downscaling method in quantifying the impact of climate change on hydrology, Journal of Hydrology, 401, 190–202, https://doi.org/10.1016/j.jhydrol.2011.02.020, 2011.

700

Compagno, L., Zekollari, H., Huss, M., and Farinotti, D.: Limited impact of climate forcing products on future glacier evolution in Scandinavia and Iceland, J. Glaciol., 67, 727–743, https://doi.org/10.1017/jog.2021.24, 2021.

Condom, T., Martínez, R., Pabón, J. D., Costa, F., Pineda, L., Nieto, J. J., López, F., and Villacis, M.: Climatological and Hydrological Observations for the South American Andes: In situ Stations, Satellite, and Reanalysis Data Sets, Frontiers in Earth Science, 8, 1–20, https://doi.org/10.3389/feart.2020.00092, 2020.

Davies, B. J. and Glasser, N. F.: Accelerating shrinkage of Patagonian glaciers from the Little Ice Age (∼AD 1870) to 2011, Journal of Glaciology, 58, 1063–1084, https://doi.org/10.3189/2012JoG12J026, 2012.

Drenkhan, F., Buytaert, W., Mackay, J. D., Barrand, N. E., Hannah, D. M., and Huggel, C.: Looking beyond glaciers to understand mountain water security, Nat Sustain, 6, 130–138, https://doi.org/10.1038/s41893-022-00996-4, 2022.

Dussaillant, I., Berthier, E., Brun, F., Masiokas, M., Hugonnet, R., Favier, V., Rabatel, A., Pitte, P., and Ruiz, L.: Two decades of glacier mass loss along the Andes, Nature Geoscience, 1–7, https://doi.org/10.1038/s41561-019-0432-5, 2019.

Eyring, V., Bony, S., Meehl, G. A., Senior, C. A., Stevens, B., Stouffer, R. J., and Taylor, K. E.: Overview of the Coupled Model Intercomparison Project Phase 6 (CMIP6) experimental design and organization, Geoscientific Model Development, 9, 1937–1958, https://doi.org/10.5194/gmd-9-1937-2016, 2016.

Farinotti, D., Huss, M., Fürst, J. J., Landmann, J., Machguth, H., Maussion, F., and Pandit, A.: A consensus estimate for the ice thickness distribution of all glaciers on Earth, Nat. Geosci., 12, 168–173, https://doi.org/10.1038/s41561-019-0300-3, 2019.

Gabbi, J., Farinotti, D., Bauder, A., and Maurer, H.: Ice volume distribution and implications on runoff projections in a glacierized catchment, Hydrology and Earth System Sciences, 16, 4543–4556, https://doi.org/10.5194/hess-16-4543-2012, 2012.

Garreaud, R. D., Alvarez-Garreton, C., Barichivich, J., Boisier, J. P., Christie, D., Galleguillos, M., LeQuesne, C., McPhee, J., Zambrano-Bigiarini, M., Pablo Boisier, J., Christie, D., Galleguillos, M., LeQuesne, C., McPhee, J., and Zambrano-Bigiarini, M.: The 2010–2015 megadrought in central Chile: impacts on regional hydroclimate and vegetation, Hydrology and Earth System Sciences, 21, 6307–6327, https://doi.org/10.5194/hess-21-6307-2017, 2017.

Gateño, F., Mendoza, P. A., Vásquez, N., Lagos-Zúñiga, M., Jiménez, H., Jerez, C., Vargas, X., Rubio-Álvarez, E., and Montserrat, S.: Screening CMIP6 models for Chile based on past performance and code genealogy, Climatic Change, 177, 87, https://doi.org/10.1007/s10584-024-03742-1, 2024.

Hanus, S., Schuster, L., Burek, P., Maussion, F., Wada, Y., and Viviroli, D.: Coupling a large-scale glacier and hydrological model (OGGM v1.5.3 and CWatM V1.08) – Towards an improved representation of mountain water resources in global assessments, https://doi.org/10.5194/egusphere-2023-2562, 22 January 2024.

Hausfather, Z., Marvel, K., Schmidt, G. A., Nielsen-Gammon, J. W., and Zelinka, M.: Climate simulations: recognize the 'hot model' problem, Nature, 605, 26–29, https://doi.org/10.1038/d41586-022-01192-2, 2022.

Hersbach, H., Bell, B., Berrisford, P., Hirahara, S., Horányi, A., Muñoz-Sabater, J., Nicolas, J., Peubey, C., Radu, R., Schepers, D., Simmons, A., Soci, C., Abdalla, S., Abellan, X., Balsamo, G., Bechtold, P., Biavati, G., Bidlot, J., Bonavita, M., De Chiara, G., Dahlgren, P., Dee, D., Diamantakis, M., Dragani, R., Flemming, J., Forbes, R., Fuentes, M., Geer, A., Haimberger, L., Healy, S., Hogan, R. J., Hólm, E., Janisková, M., Keeley, S., Laloyaux, P., Lopez, P., Lupu, C., Radnoti, G., de Rosnay, P., Rozum, I., Vamborg, F., Villaume, S., and Thépaut, J.-N.: The ERA5 global reanalysis, Quarterly Journal of the Royal Meteorological Society, 146, 1999–2049, https://doi.org/10.1002/qj.3803, 2020.

Hock, R., Maussion, F., Marzeion, B., and Nowicki, S.: What is the global glacier ice volume outside the ice sheets?, J. Glaciol., 69, 204–210, https://doi.org/10.1017/jog.2023.1, 2023.

740   Hugonnet, R., McNabb, R., Berthier, E., Menounos, B., Nuth, C., Girod, L., Farinotti, D., Huss, M., Dussaillant, I., Brun, F., and Kääb, A.: Accelerated global glacier mass loss in the early twenty-first century, Nature, 592, 726–731, https://doi.org/10.1038/s41586-021-03436-z, 2021.

Huss, M. and Hock, R.: A new model for global glacier change and sea-level rise, Frontiers in Earth Science, 3, 1–22, https://doi.org/10.3389/feart.2015.00054, 2015.

745   Huss, M. and Hock, R.: Global-scale hydrological response to future glacier mass loss, Nature Climate Change, 8, 135–140, https://doi.org/10.1038/s41558-017-0049-x, 2018.

Huss, M., Zemp, M., Joerg, P. C., and Salzmann, N.: High uncertainty in 21st century runoff projections from glacierized basins, Journal of Hydrology, 510, 35–48, https://doi.org/10.1016/j.jhydrol.2013.12.017, 2014.

Huss, M., Bookhagen, B., Huggel, C., Jacobsen, D., Bradley, R. s., Clague, J. j., Vuille, M., Buytaert, W., Cayan, D. r., 750   Greenwood, G., Mark, B. g., Milner, A. m., Weingartner, R., and Winder, M.: Toward mountains without permanent snow and ice, Earth's Future, 5, 418–435, https://doi.org/10.1002/2016EF000514, 2017.

Immerzeel, W. W., Lutz, A. F., Andrade, M., Bahl, A., Biemans, H., Bolch, T., Hyde, S., Brumby, S., Davies, B. J., Elmore, A. C., Emmer, A., Feng, M., Fernández, A., Haritashya, U., Kargel, J. S., Koppes, M., Kraaijenbrink, P. D. A., Kulkarni, A. V., Mayewski, P. A., Nepal, S., Pacheco, P., Painter, T. H., Pellicciotti, F., Rajaram, H., Rupper, S., Sinisalo, A., Shrestha, A. 755   B., Viviroli, D., Wada, Y., Xiao, C., Yao, T., and Baillie, J. E. M.: Importance and vulnerability of the world's water towers, Nature, 577, 364–369, https://doi.org/10.1038/s41586-019-1822-y, 2020.

IPCC: High Mountain Areas, in: The Ocean and Cryosphere in a Changing Climate: Special Report of the Intergovernmental Panel on Climate Change, Cambridge, https://doi.org/10.1017/9781009157964.004, 2022.

Iriarte, J. L., Pantoja, S., and Daneri, G.: Oceanographic Processes in Chilean Fjords of Patagonia: From small to large-scale 760   studies, Progress in Oceanography, 129, 1–7, https://doi.org/10.1016/j.pocean.2014.10.004, 2014.

Iturbide, M., Fernández, J., Gutiérrez, J. M., Bedia, J., Cimadevilla, E., Díez-Sierra, J., Manzanas, R., Casanueva, A., Baño-Medina, J., Milovac, J., Herrera, S., Cofiño, A. S., San Martín, D., García-Díez, M., Hauser, M., Huard, D., and Yelekci, Ö.: Repository supporting the implementation of FAIR principles in the IPCC-WGI Atlas, , https://doi.org/10.5281/ZENODO.3691645, 2021.

765   Kaser, G., Großhauser, M., and Marzeion, B.: Contribution potential of glaciers to water availability in different climate regimes, Proceedings of the National Academy of Sciences, 107, 20223–20227, https://doi.org/10.1073/pnas.1008162107, 2010.

Lange, S.: ISIMIP3b bias adjustment fact sheet, 2021.

Li, F., Maussion, F., Wu, G., Chen, W., Yu, Z., Li, Y., and Liu, G.: Influence of glacier inventories on ice thickness estimates 770   and future glacier change projections in the Tian Shan range, Central Asia, J. Glaciol., 1–15, https://doi.org/10.1017/jog.2022.60, 2022.

Logan, T., Aoun, A., Bourgault, P., Dupuis, É., Huard, D., Lavoie, J., Rondeau-Genesse, G., Smith, T. J., Alegre, R., Barnes, C., Biner, S., Caron, D., Ehbrecht, C., Fyke, J., Keel, T., Labonté, M.-P., Lierhammer, L., Low, J.-F., Quinn, J., Roy, P., Squire, D., Stephens, A., Tanguy, M., and Whelan, C.: Ouranosinc/xclim: v0.39.0, , https://doi.org/10.5281/zenodo.7274811, 2022.

775 Mackay, J. D., Barrand, N. E., Hannah, D. M., Krause, S., Jackson, C. R., Everest, J., Aðalgeirsdóttir, G., and Black, A. R.: Future evolution and uncertainty of river flow regime change in a deglaciating river basin, Hydrol. Earth Syst. Sci., 23, 1833–1865, https://doi.org/10.5194/hess-23-1833-2019, 2019.

Malles, J., Maussion, F., Ultee, L., Kochtitzky, W., Copland, L., and Marzeion, B.: Exploring the impact of a frontal ablation parameterization on projected 21st-century mass change for Northern Hemisphere glaciers, Journal of Glaciology, 2023.

780 Marzeion, B., Jarosch, A. H., and Hofer, M.: Past and future sea-level change from the surface mass balance of glaciers, The Cryosphere, 6, 1295–1322, https://doi.org/10.5194/tc-6-1295-2012, 2012.

Marzeion, B., Hock, R., Anderson, B., Bliss, A., Champollion, N., Fujita, K., Huss, M., Immerzeel, W. W., Kraaijenbrink, P., Malles, J., Maussion, F., Radić, V., Rounce, D. R., Sakai, A., Shannon, S., van de Wal, R., and Zekollari, H.: Partitioning the Uncertainty of Ensemble Projections of Global Glacier Mass Change, Earth's Future, 8,
785 https://doi.org/10.1029/2019EF001470, 2020.

Masiokas, M., Rabatel, A., Rivera, A., Ruiz, L., Pitte, P., Ceballos, J. L., Barcaza, G., Soruco, A., and Bown, F.: A review of the current state and recent changes of the Andean cryosphere, Frontiers in Earth Science, 8, 99, https://doi.org/10.3389/FEART.2020.00099, 2020.

Masiokas, M. H., Cara, L., Villalba, R., Pitte, P., Luckman, B. H., Toum, E., Christie, D. A., Le Quesne, C., and Mauget, S.:
790 Streamflow variations across the Andes (18°–55°S) during the instrumental era, Scientific Reports, 9, 17879, https://doi.org/10.1038/s41598-019-53981-x, 2019.

Maussion, F., Butenko, A., Champollion, N., Dusch, M., Eis, J., Fourteau, K., Gregor, P., Jarosch, A. H., Landmann, J., Oesterle, F., Recinos, B., Rothenpieler, T., Vlug, A., Wild, C. T., and Marzeion, B.: The Open Global Glacier Model (OGGM) v1.1, Geoscientific Model Development, 12, 909–931, https://doi.org/10.5194/gmd-12-909-2019, 2019.

795 McCarthy, M., Meier, F., Fatichi, S., Stocker, B. D., Shaw, T. E., Miles, E., Dussaillant, I., and Pellicciotti, F.: Glacier Contributions to River Discharge During the Current Chilean Megadrought, Earth's Future, 10, e2022EF002852, https://doi.org/10.1029/2022EF002852, 2022.

McMillan, H. K.: A review of hydrologic signatures and their applications, WIREs Water, 8, e1499, https://doi.org/10.1002/wat2.1499, 2021.

800 Mernild, S. H., Liston, G. E., Hiemstra, C., and Wilson, R.: The Andes Cordillera. Part III: glacier surface mass balance and contribution to sea level rise (1979–2014), International Journal of Climatology, 37, 3154–3174, https://doi.org/10.1002/joc.4907, 2017.

Millan, R., Rignot, E., Rivera, A., Martineau, V., Mouginot, J., Zamora, R., Uribe, J., Lenzano, G., De Fleurian, B., Li, X., Gim, Y., and Kirchner, D.: Ice Thickness and Bed Elevation of the Northern and Southern Patagonian Icefields, Geophysical
805 Research Letters, https://doi.org/10.1029/2019GL082485, 2019.

Millan, R., Mouginot, J., Rabatel, A., and Morlighem, M.: Ice velocity and thickness of the world's glaciers, Nat. Geosci., 15, 124–129, https://doi.org/10.1038/s41561-021-00885-z, 2022.

Milner, A. M., Khamis, K., Battin, T. J., Brittain, J. E., Barrand, N. E., Füreder, L., Cauvy-Frauni, S., Gíslason, G. M., Jacobsen, D., Hannah, D. M., Hodson, A. J., Hood, E., Lencioni, V., Ólafsson, J. S., Robinson, C. T., Tranter, M., and Brown, L. E.: Glacier shrinkage driving global changes in downstream systems, Proceedings of the National Academy of Sciences, 114, 9770–9778, https://doi.org/10.1073/pnas.1619807114, 2017.

Minowa, M., Schaefer, M., Sugiyama, S., Sakakibara, D., and Skvarca, P.: Frontal ablation and mass loss of the Patagonian icefields, Earth and Planetary Science Letters, 561, 116811, https://doi.org/10.1016/j.epsl.2021.116811, 2021.

Morales, M. S., Cook, E. R., Barichivich, J., Christie, D. A., Villalba, R., LeQuesne, C., Srur, A. M., Ferrero, M. E., González-Reyes, Á., Couvreux, F., Matskovsky, V., Aravena, J. C., Lara, A., Mundo, I. A., Rojas, F., Prieto, M. R., Smerdon, J. E., Bianchi, L. O., Masiokas, M. H., Urrutia-Jalabert, R., Rodriguez-Catón, M., Muñoz, A. A., Rojas-Badilla, M., Alvarez, C., Lopez, L., Luckman, B. H., Lister, D., Harris, I., Jones, P. D., Williams, A. P., Velazquez, G., Aliste, D., Aguilera-Betti, I., Marcotti, E., Flores, F., Muñoz, T., Cuq, E., and Boninsegna, J. A.: Six hundred years of South American tree rings reveal an increase in severe hydroclimatic events since mid-20th century, Proceedings of the National Academy of Sciences, 117, 16816–16823, https://doi.org/10.1073/pnas.2002411117, 2020.

NASA JPL: NASADEM Merged DEM Global 1 arc second V001 [Data set], 2020.

O'Neill, B. C., Tebaldi, C., van Vuuren, D. P., Eyring, V., Friedlingstein, P., Hurtt, G., Knutti, R., Kriegler, E., Lamarque, J.-F., Lowe, J., Meehl, G. A., Moss, R., Riahi, K., and Sanderson, B. M.: The Scenario Model Intercomparison Project (ScenarioMIP) for CMIP6, Geosci. Model Dev., 9, 3461–3482, https://doi.org/10.5194/gmd-9-3461-2016, 2016.

Pasquini, A., Cosentino, N., and Depetris, P.: The Main Hydrological Features of Patagonia's Santa Cruz River: An Updated Assessment, 195–210, https://doi.org/10.1007/978-3-030-89676-8_9, 2021.

Pedregosa, F., Varoquaux, G., Gramfort, A., Michel, V., Thirion, B., Grisel, O., Blondel, M., Prettenhofer, P., Weiss, R., Dubourg, V., Vanderplas, J., Passos, A., Cournapeau, D., Brucher, M., Perrot, M., and Duchesnay, É.: Scikit-learn: Machine Learning in Python, Journal of Machine Learning Research, 12, 2825–2830, 2011.

Pesci, M. H., Schulte Overberg, P., Bosshard, T., and Förster, K.: From global glacier modeling to catchment hydrology: bridging the gap with the WaSiM-OGGM coupling scheme, Frontiers in Water, 5, 2023.

Poff, N. L., Allan, J. D., Bain, M. B., Karr, J. R., Prestegaard, K. L., Richter, B. D., Sparks, R. E., and Stromberg, J. C.: The Natural Flow Regime, BioScience, 47, 769–784, https://doi.org/10.2307/1313099, 1997.

Pritchard, H. D.: Asia's shrinking glaciers protect large populations from drought stress, Nature, 569, 649–654, https://doi.org/10.1038/s41586-019-1240-1, 2019.

Rasul, G. and Molden, D.: The Global Social and Economic Consequences of Mountain Cryospheric Change, Frontiers in Environmental Science, 7, 2019.

RGI Consortium: Randolph Glacier Inventory - A Dataset of Global Glacier Outlines, Version 6, https://doi.org/10.7265/4M1F-GD79, 2017.

RGI Consortium: Randolph Glacier Inventory - A Dataset of Global Glacier Outlines, Version 7, https://doi.org/10.5067/F6JMOVY5NAVZ, 2023.

Richter, B. D., Baumgartner, J. V., Powell, J., and Braun, D. P.: A Method for Assessing Hydrologic Alteration within Ecosystems, Conservation Biology, 10, 1163–1174, https://doi.org/10.1046/j.1523-1739.1996.10041163.x, 1996.

845 Rounce, D. R., Khurana, T., Short, M. B., Hock, R., Shean, D. E., and Brinkerhoff, D. J.: Quantifying parameter uncertainty in a large-scale glacier evolution model using Bayesian inference: application to High Mountain Asia, J. Glaciol., 66, 175–187, https://doi.org/10.1017/jog.2019.91, 2020.

Rounce, D. R., Hock, R., Maussion, F., Hugonnet, R., Kochtitzky, W., Huss, M., Berthier, E., Brinkerhoff, D., Compagno, L., Copland, L., Farinotti, D., Menounos, B., and McNabb, R. W.: Global glacier change in the 21st century: Every increase in temperature matters, Science, 379, 78–83, https://doi.org/10.1126/science.abo1324, 2023.

850 Ruiz, L., Pitte, P., Rivera, A., Schaefer, M., and Masiokas, M. H.: Current State and Recent Changes of Glaciers in the Patagonian Andes (~37 °S to 55 °S), in: Freshwaters and Wetlands of Patagonia: Ecosystems and Socioecological Aspects, edited by: Mataloni, G. and Quintana, R. D., Springer International Publishing, Cham, 59–91, https://doi.org/10.1007/978-3-031-10027-7_4, 2022.

Sauter, T.: Revisiting extreme precipitation amounts over southern South America and implications for the Patagonian 855 Icefields, Hydrology and Earth System Sciences, 24, 2003–2016, https://doi.org/10.5194/hess-24-2003-2020, 2020.

Schmidt, L., Heße, F., Attinger, S., and Kumar, R.: Challenges in Applying Machine Learning Models for Hydrological Inference: A Case Study for Flooding Events Across Germany, Water Resources Research, 56, e2019WR025924, https://doi.org/10.1029/2019WR025924, 2020.

Schuster, L., Rounce, D. R., and Maussion, F.: Glacier projections sensitivity to temperature-index model choices and 860 calibration strategies, Ann. Glaciol., 1–16, https://doi.org/10.1017/aog.2023.57, 2023.

Somers, L. D., McKenzie, J. M., Mark, B. G., Lagos, P., Ng, G. C., Wickert, A. D., Yarleque, C., Baraër, M., and Silva, Y.: Groundwater Buffers Decreasing Glacier Melt in an Andean Watershed—But Not Forever, Geophysical Research Letters, 46, 13016–13026, https://doi.org/10.1029/2019GL084730, 2019.

Svetnik, V., Liaw, A., Tong, C., Culberson, J. C., Sheridan, R. P., and Feuston, B. P.: Random Forest: A Classification and 865 Regression Tool for Compound Classification and QSAR Modeling, Journal of Chemical Information and Computer Sciences, 43, 1947–1958, https://doi.org/10.1021/ci034160g, 2003.

Tang, G., Clark, M. P., and Papalexiou, S. M.: EM-Earth: The Ensemble Meteorological Dataset for Planet Earth, Bulletin of the American Meteorological Society, 103, E996–E1018, https://doi.org/10.1175/BAMS-D-21-0106.1, 2022.

Tang, G., Clark, M. P., Knoben, W. J. M., Liu, H., Gharari, S., Arnal, L., Beck, H. E., Wood, A. W., Newman, A. J., and 870 Papalexiou, S. M.: The Impact of Meteorological Forcing Uncertainty on Hydrological Modeling: A Global Analysis of Cryosphere Basins, Water Resources Research, 59, e2022WR033767, https://doi.org/10.1029/2022WR033767, 2023.

Tarek, M., Brissette, F., and Arsenault, R.: Uncertainty of gridded precipitation and temperature reference datasets in climate change impact studies, Hydrol. Earth Syst. Sci., 25, 3331–3350, https://doi.org/10.5194/hess-25-3331-2021, 2021.

Temme, F., Farías-Barahona, D., Seehaus, T., Jaña, R., Arigony-Neto, J., Gonzalez, I., Arndt, A., Sauter, T., Schneider, C., 875 and Fürst, J. J.: Strategies for regional modeling of surface mass balance at the Monte Sarmiento Massif, Tierra del Fuego, The Cryosphere, 17, 2343–2365, https://doi.org/10.5194/tc-17-2343-2023, 2023.

Tokarska, K. B., Stolpe, M. B., Sippel, S., Fischer, E. M., Smith, C. J., Lehner, F., and Knutti, R.: Past warming trend constrains future warming in CMIP6 models, Science Advances, 6, eaaz9549, https://doi.org/10.1126/sciadv.aaz9549, 2020.

880 Ultee, L., Coats, S., and Mackay, J.: Glacial runoff buffers droughts through the 21st century, Earth System Dynamics, 13, 935–959, https://doi.org/10.5194/esd-13-935-2022, 2022.

Van Tiel, M., Stahl, K., Freudiger, D., and Seibert, J.: Glacio-hydrological model calibration and evaluation, WIREs Water, 7, e1483, https://doi.org/10.1002/wat2.1483, 2020.

Van Tiel, M., Van Loon, A. F., Seibert, J., and Stahl, K.: Hydrological response to warm and dry weather: do glaciers compensate?, Hydrology and Earth System Sciences, 25, 3245–3265, https://doi.org/10.5194/hess-25-3245-2021, 2021.

885 Van Tiel, M., Weiler, M., Freudiger, D., Moretti, G., Kohn, I., Gerlinger, K., and Stahl, K.: Melting Alpine Water Towers Aggravate Downstream Low Flows: A Stress-Test Storyline Approach, Earth's Future, 11, e2022EF003408, https://doi.org/10.1029/2022EF003408, 2023.

Viviroli, D., Kummu, M., Meybeck, M., Kallio, M., and Wada, Y.: Increasing dependence of lowland populations on mountain water resources, Nat Sustain, 3, 917–928, https://doi.org/10.1038/s41893-020-0559-9, 2020.

890 Vries, M. V. W. de, Romero, M., Penprase, S. B., Ng, G.-H. C., and Wickert, A. D.: Increasing rate of 21st century volume loss of the Patagonian Icefields measured from proglacial river discharge, Journal of Glaciology, 1–16, https://doi.org/10.1017/jog.2023.9, 2023.

Wang, H., Chen, J., Xu, C., Zhang, J., and Chen, H.: A Framework to Quantify the Uncertainty Contribution of GCMs Over Multiple Sources in Hydrological Impacts of Climate Change, Earth's Future, 8, https://doi.org/10.1029/2020EF001602, 2020.

895 Watanabe, M., Yanagawa, A., Watanabe, S., Hirabayashi, Y., and Kanae, S.: Quantifying the range of future glacier mass change projections caused by differences among observed past-climate datasets, Clim Dyn, 53, 2425–2435, https://doi.org/10.1007/s00382-019-04868-0, 2019.

Werder, M. A., Huss, M., Paul, F., Dehecq, A., and Farinotti, D.: A Bayesian ice thickness estimation model for large-scale applications, Journal of Glaciology, 66, 137–152, https://doi.org/10.1017/jog.2019.93, 2020.

900 Zalazar, L., Ferri, L., Castro, M., Gargantini, H., Gimenez, M., Pitte, P., Ruiz, L., Masiokas, M., Costa, G., and Villalba, R.: Spatial distribution and characteristics of Andean ice masses in Argentina: results from the first National Glacier Inventory, Journal of Glaciology, 66, 938–949, https://doi.org/10.1017/jog.2020.55, 2020.

Zambrano-Bigiarini, M.: Temporal and spatial evaluation of long-term satellite-based precipitation products across the complex topographical and climatic gradients of Chile, in: Remote Sensing and Modeling of the Atmosphere, Oceans, and Interactions VII, Remote Sensing and Modeling of the Atmosphere, Oceans, and Interactions VII, 905 https://doi.org/10.1117/12.2513645, 2018.

Zekollari, H., Huss, M., and Farinotti, D.: Modelling the future evolution of glaciers in the European Alps under the EURO-CORDEX RCM ensemble, The Cryosphere, 13, 1125–1146, https://doi.org/10.5194/tc-13-1125-2019, 2019.

Zekollari, H., Huss, M., Farinotti, D., and Lhermitte, S.: Ice-Dynamical Glacier Evolution Modeling—A Review, Reviews of 910 Geophysics, 60, e2021RG000754, https://doi.org/10.1029/2021RG000754, 2022.

Zekollari, H., Huss, M., Schuster, L., Maussion, F., Rounce, D. R., Aguayo, R., Champollion, N., Compagno, L., Hugonnet, R., Marzeion, B., Mojtabavi, S., and Farinotti, D.: 21st century global glacier evolution under CMIP6 scenarios and the role of glacier-specific observations, EGUsphere, 1–33, https://doi.org/10.5194/egusphere-2024-1013, 2024.

Zhao, H., Su, B., Lei, H., Zhang, T., and Xiao, C.: A new projection for glacier mass and runoff changes over High Mountain Asia, Science Bulletin, 68, 43–47, https://doi.org/10.1016/j.scib.2022.12.004, 2023.

915